Deformation of the Early Glaucomatous Monkey Optic Nerve Head Connective Tissue after Acute IOP Elevation in 3-D Histomorphometric Reconstructions

Hongli Yang,[1] Hilary Thompson,[2] Michael D. Roberts,[3] Ian A. Sigal,[3] J. Crawford Downs,[3] and Claude F. Burgoyne[1]

Purpose. To retest the hypothesis that monkey ONH connective tissues become hypercompliant in early experimental glaucoma (EEG), by using 3-D histomorphometric reconstructions, and to expand the characterization of EEG connective tissue deformation to nine EEG eyes.

Methods. Trephinated ONH and peripapillary sclera from both eyes of nine monkeys that were perfusion fixed, with one normal eye at IOP 10 mm Hg and the other EEG eye at 10 (n = 3), 30 (n = 3), or 45 (n = 3) mm Hg were serial sectioned, 3-D reconstructed, 3-D delineated, and quantified with 3-D reconstruction techniques developed in prior studies by the authors. Overall, and for each monkey, intereye differences (EEG eye minus normal eye) for each parameter were calculated and compared by ANOVA. Hypercompliance in the EEG 30 and 45 eyes was assessed by ANOVA, and deformations in all nine EEG eyes were separately compared by region without regard for fixation IOP.

Results. Hypercompliant deformation was not significant in the overall ANOVA, but was suggested in a subset of EEG 30/45 eyes. EEG eye deformations included posterior laminar deformation, neural canal expansion, lamina cribrosa thickening, and posterior (outward) bowing of the peripapillary sclera. Maximum posterior laminar deformation and scleral canal expansion co-localized to either the inferior nasal or superior temporal quadrants in the eyes with the least deformation and involved both quadrants in the eyes achieving the greatest deformation.

Conclusions. The data suggest that, in monkey EEG, ONH connective tissue hypercompliance may occur only in a subset of eyes and that early ONH connective tissue deformation is maximized in the superior temporal and/or inferior nasal quadrants. (*Invest Ophthalmol Vis Sci.* 2011;52:345–363) DOI: 10.1167/iovs.09-5122

In the monkey model of unilateral early experimental glaucoma (EEG), chronic, laser-induced intraocular pressure (IOP) elevation is induced in one eye of an animal, whereas the contralateral eye is maintained as the normal control.[1–8] Early glaucomatous damage in the treated eye is defined as the onset of confocal scanning laser tomography (CSLT)–detected surface change that is not present in the contralateral normal eye. Monkeys are then perfusion fixed with either both eyes at manometer-controlled IOPs of 10 mm Hg (EEG 10/10 monkeys) or with the normal eye at IOP 10 mm Hg and the EEG eye at IOP of 30 or 45 mm Hg (EEG 10/30 and 10/45 monkeys). Postmortem histomorphometric analyses[9–11] are then performed in which the differences between the EEG and control eyes are assumed to be due to fixed or permanent neural and connective tissue deformation in EEG eyes of the EEG 10/10 animals, or a combination of permanent and acute deformation in the EEG eyes of the EEG 10/30 and 10/45 animals. We defined *fixed* or *permanent* deformation as deformation that is not reversible by lowering IOP to 10 mm Hg and is the likely result of a combination of connective tissue yield or failure and active connective tissue remodeling. We defined *acute deformation* as elastic deformation that is reversible by lowering IOP to 10 mm Hg.

In a previous study,[12] we cut 16 immersion-fixed and 18 perfusion-fixed monkey optic nerve heads (ONHs) into serial 4-μm sagittal histologic sections and measured anterior laminar position and thickness and scleral canal diameter in digitized images of every sixth section for a rigorous study of the 2-D architecture of the lamina cribrosa (LC) and anterior scleral canal wall in normal and EEG monkey eyes at various levels of IOP. The principal findings of that report were that permanent or fixed posterior deformation of the LC, an increase in laminar thickness, and an enlargement of the anterior scleral canal opening were present at this stage of EEG damage, and that these fixed components of damage were accompanied by hypercompliant deformation of the LC in the group of EEG eyes fixed at IOP 30 and 45 mm Hg.

The first goal of the present study was to retest the hypothesis that the ONH connective tissues are altered by early glaucomatous damage in such a way that they become hypercompliant, by using our current technique for 3-D histomorphometric reconstruction,[9–11,13–15] which allows the resultant reconstructions to eventually undergo finite element modeling.[16,17] EEG eye hypercompliance is important because it suggests that not just the architecture,[9–12] but also the material properties[18,19] (Girard MJ, et al. *IOVS* 2009;50:ARVO E-Abstract 5217) of ONH connective tissues are altered by chronic exposure to moderate levels of elevated IOP.

From the [1]Optic Nerve Head Research Laboratory and [3]Ocular Biomechanics Laboratory, Devers Eye Institute, Legacy Health System, Portland, Oregon; and the [2]School of Public Health, Louisiana State University Health Sciences Center, New Orleans, Louisiana.

Supported in part by USPHS Grants R01EY011610 (CFB) from the National Eye Institute, National Institutes of Health, Bethesda, Maryland; a grant from the American Health Assistance Foundation, Rockville, Maryland (CFB); a grant from The Whitaker Foundation, Arlington, Virginia (CFB); a Career Development Award from Research to Prevent Blindness (CFB); The Legacy Good Samaritan Foundation, Portland, Oregon; and the Sears Trust for Biomedical Research, Mexico, Missouri.

Submitted for publication December 23, 2009; revised June 4, 2010; accepted June 22, 2010.

Disclosure: **H. Yang**, None; **H. Thompson**, None; **M.D. Roberts**, None; **I.A. Sigal**, None; **J.C. Downs**, None; **C.F. Burgoyne**, None

Corresponding author: Claude F. Burgoyne, Optic Nerve Head Research Laboratory, Devers Eye Institute, 1225 NE 2nd Avenue, PO Box 3950, Portland OR 97208-3950; cfburgoyne@deverseye.org.

Table 1. Animal and Eye Data

Monkey						IOP (mm Hg)				State of Eye at Perfusion		Axial Length (mm)		Histomorphometric Optic Disc Size#			
No.	ID	Weight (kg)	Age (y)	Species	Eye	Normal (Prelaser)*	Maximum (Postlaser)	Cumulative IOP (mm Hg Days)†	Postlaser MPD Change (μm)‡	Condition	IOP (mm Hg)§	Normal (Prelaser)‖	Immediately Before Death¶	Serial Section Images (n)	Vertical (μm)	Horizontal (μm)	Area (mm^2)
1	AA3K	7.18	8	Cyno	Left	13	—	—	—	Normal	10	20.92	21.16	320	1595	1106	1.385
					Right	12	23	63	−74	EEG	30	21.04	21.37	290	1681	1062	1.402
2	5644	7.8	6	Rhesus	Right	11	—	—	—	Normal	10	21.12	21.01	227	1474	1133	1.312
					Left	9	26	272	−112	EEG	45	20.82	21.73	356	1529	1140	1.369
3	300	6.8	10	Rhesus	Right	10	—	—	—	Normal	10	19.78	19.79	183	1363	989	1.059
					Left	14	16	237	−112	EEG	30	19.78	20.1	213	1433	1035	1.165
4	AA40	7.62	8.1	Cyno	Left	11	—	—	—	Normal	10	19.26	19.24	237	1365	1004	1.360
					Right	9	37	360	−142	EEG	10	19.9	19.6	249	1363	1005	1.356
5	AA4C	7.52	8.3	Cyno	Right	8	—	—	—	Normal	10	20.06	19.4	222	1453	1045	1.323
					Left	9	20	116	−134	EEG	10	20.19	20.4	238	1463	1106	1.391
6	AA3G	8.24	8	Cyno	Left	11	—	—	—	Normal	10	19.97	20.06	290	1267	889	0.885
					Right	11	36	338	−214	EEG	45	20.04	20.48	280	1455	1051	1.201
7	AA37	8.18	8.3	Cyno	Right	10	—	—	—	Normal	10	19.69	19.79	290	1337	1032	1.296
					Left	10	26	186	−133	EEG	10	19.83	20.08	411	1489	1068	1.394
8	514	6.0	5	Rhesus	Right	8	—	—	—	Normal	10	20.48	20.43	250	1459	1043	1.195
					Left	8	29	50	−115	EEG	30	20.45	20.83	313	1614	1117	1.416
9	7489	5.75	11	Rhesus	Right	8	—	—	—	Normal	10	20.9	20.87	240	1737	1263	1.722
					Left	8	38	807	−172	EEG	45	20.76	22.46	337	1765	1308	1.813

* Prelaser IOPs are the mean IOPs of the three to nine baseline measurements in monkeys under ketamine/xylazine anesthesia.

† The difference in area under the IOP time curve between the EEG and normal eye (see Fig. 1).

‡ The difference between the postlaser minimum MPD and the mean of the baseline MPD in the treated eye.

§ High pressure (30 or 45 mm Hg) was applied to six EEG eyes for 15 minutes before death.

‖ Baseline axial length measured during the first baseline compliance testing session.

¶ Predeath axial length measured during the final compliance testing session.

Optic disc dimension as determined by the clinical visible optic disc margin, which is Bruch's membrane opening or the NCO in these eyes at the perfusion pressure. Vertical length as determined by the major length of the NCO ellipse; horizontal length as determined by the minor length of the NCO ellipse; disc area is determined by the area of the NCO ellipse.

To retest this hypothesis, we three-dimensionally characterized the magnitude of intereye ONH connective tissue differences in a new group of three EEG 10/10, three EEG 10/30, and three EEG 10/45 monkeys. To characterize the range of fixed or permanent deformation in a previous report,[14] we compared the differences between the EEG and normal eyes of each EEG 10/10 monkey to the magnitude of intereye ONH connective tissue differences in a group of bilaterally normal monkeys that had been perfusion fixed with both eyes at IOP 10 (N 10/10 animals). To assess for the presence of hypercompliance in the EEG eyes of the EEG 10/30 and 10/45 animals, we designed the present study to compare the magnitude of the intereye differences in these animals to the magnitude of fixed deformation in the EEG 10/10 animals and the intereye differences in a separate group of bilaterally normal 10/30 and 10/45 animals that were, themselves, the subject of a recent report.[15]

However, because in clinical practice the level of IOP is not always fixed at IOP 10 mm Hg and pressures of 30 and 45 mm Hg are well in the range of untreated human[20–25]and monkey (experimental) glaucoma,[1,7,12,26,27] a second goal of this study was to expand our initial 2-D[12] and 3-D[9–11,13–15] characterization of early glaucomatous connective tissue deformation to include the six EEG eyes from the 10/30 and 10/45 animals from this study without regard for the level of IOP in the EEG eyes at the time of fixation. The study groups and the abbreviations used herein are listed inAppendix Table A1.

Materials and Methods

Animals

All animals were treated in accordance with the ARVO Statement for the Use of Animals in Ophthalmic and Vision Research. Nine male adult EEG monkeys were used for the study (Table 1). The three EEG 10/10 animals have been extensively characterized in a series of reports.[9–11] To assess for the presence of hypercompliance in the six EEG 10/30 and 10/45 animals, we compared data from those animals to those of both the EEG 10/10 animals and a separate group of previously reported bilaterally normal 10/10, 10/30, and 10/45 animals.[14,15]

ONH Surface Imaging, Early Glaucoma, and Cumulative IOP Insult

We have described our CSLT-based ONH surface compliance testing strategy[12,28] using our CSLT parameter mean position of the disc (MPD). All CSLT imaging in these animals was performed using a confocal laser scanning tomograph (TopSS; Laser Diagnostics Technology [LDT], San Diego, CA). Ten ultrasonic axial length measurements (Model A1500; Sonomed, Lake Success, NY) were obtained in both eyes of each animal at the baseline time point of each compliance test[12,28] and before death.

After three to eight baseline testing sessions, one eye of each monkey was subjected to laser-induced experimental elevation of IOP, and compliance testing of both eyes was repeated at 2-week intervals until the onset of a qualitative decrease in MPD on two successive postlaser imaging sessions. Topographic change analysis (TCA; HRT 3 system software, ver. 3.1.2; Heidelberg Engineering, Heidelberg, Germany) was retrospectively performed on the longitudinal LDT data, to generate the TCA maps before death that are shown in Figure 2.

All EEG monkeys were killed in approximately 1 to 5 weeks of CSLT detection of ONH surface change (Figs. 1, 2). In the nine EEG eyes, this occurred after 2 to 18 weeks of moderate IOP elevation (Table 1). Cumulative IOP exposure was calculated for each EEG eye, as described in Figure 1.

Monkey Perfusion Fixation at Prescribed IOP

In monkeys under deep pentobarbital anesthesia, IOP in both eyes was set to 10 mm Hg by anterior chamber manometer for a minimum of 30 minutes. In the EEG 10/30 and 10/45 monkeys, although the IOP in the control eye was kept at 10 mm Hg, IOP in the treated EEG eye was then elevated to 30 or 45 mm Hg for 15 minutes.[9,12,13] All monkeys were perfusion fixed via the descending aorta with 1 L of 4% buffered hypertonic paraformaldehyde solution followed by 6 L of 5% buffered hypertonic glutaraldehyde solution. After perfusion, IOP was maintained for 1 hour, and then each eye was enucleated, all extraocular tissues were removed, and the intact anterior chamber was excised 2 to 3 mm posterior to the limbus. By gross inspection, perfusion was excellent in all six eyes of the EEG 10/10 monkeys. However, blood

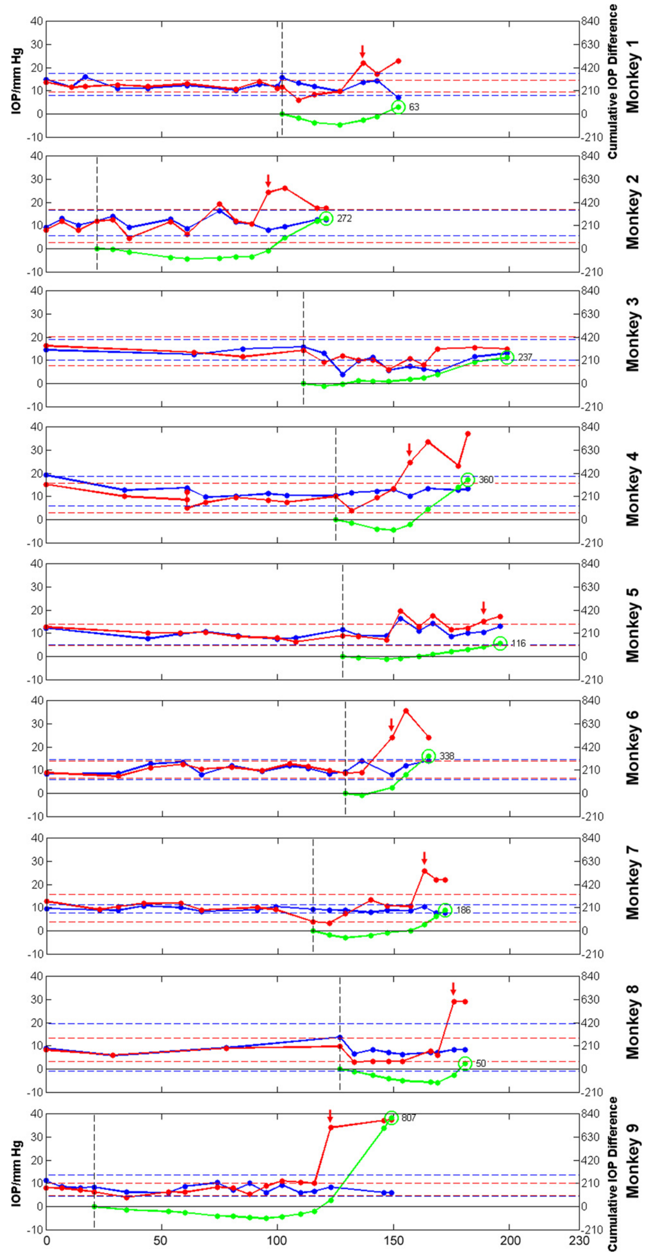

Figure 1. IOP history for both eyes of each animal and the cumulative IOP insult (mm Hg days) for each EEG eye. The cumulative IOP insult for each EEG eye (*green*) was calculated as the running difference between the area under the IOP time curve (*red*) and that of its contralateral normal eye (*blue*) after the start of lasering (*black dashed vertical line*). *Green circle*: final cumulative IOP in the EEG eyes. These data are also listed in Table 1. The 95% CIs of the baseline testing sessions were plotted for the normal eye (*blue dashed line*) and the EEG eye. *Red arrow*: first IOP outside the upper limit of the 95% CI of the baseline sessions in the EEG eye.

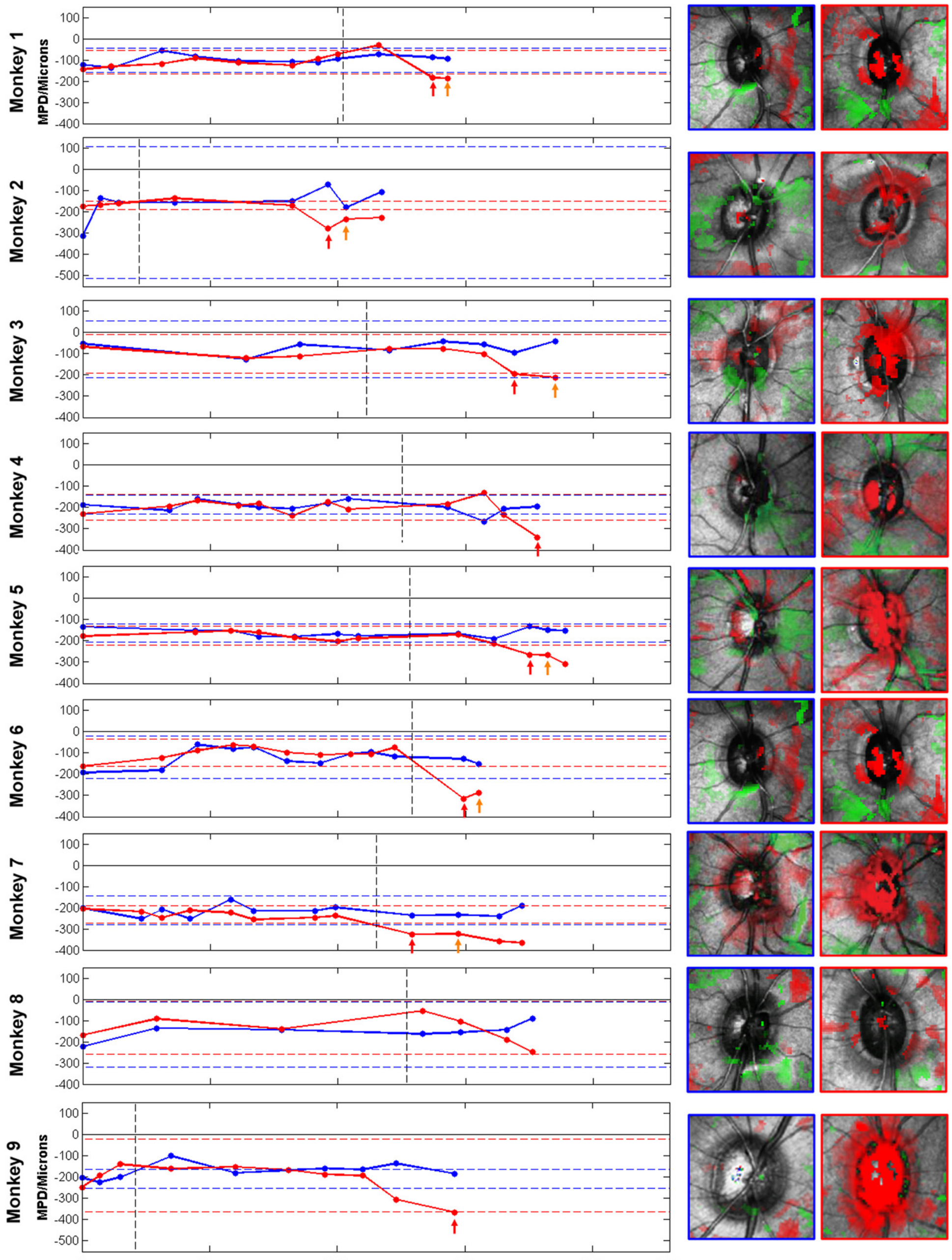

FIGURE 2. CSLT-derived MPD and TCA data for both eyes of each animal. Normal eye (*blue*) and EEG eye (*red*) MPD data (in micrometers) are plotted against time (in days) on the *left*. *Dashed black vertical line*: lasering day. The 95% CIs of the baseline testing sessions are plotted for the normal eye (*blue dashed line*) and the EEG eye (*red dashed line*). The first (*red arrow*) MPD and the second (*orange arrow*) MPD that were outside the lower limit of the 95% CI of the baseline sessions in the EEG eye are marked. The last TCA map of the normal eye (*blue border*) and the last TCA map of the EEG eye (*red border*) are on the right (in right-eye configuration) with *red* pixels representing significant retinal height decrease and *green* pixels representing significant retinal height increase from baseline. It should be noted that, although these data have been retrospectively compiled for each monkey, the decision to kill each monkey was empiric by necessity, in that the systems to rapidly process, statistically analyze, and graph the data for each monkey were not in place at the time of postlaser compliance testing of these animals.

was variably present in the retinal vessels, posterior ciliary arteries, and vortex veins of the six EEG 30/45 eyes. The posterior scleral shell with intact ONH, choroid, and retina were then placed in 5% glutaraldehyde solution for storage.

3-D Histomorphometric Reconstruction

Briefly, in each eye, the ONH and peripapillary sclera were trephinated (6-mm-diameter), pierced with alignment sutures, and embedded in paraffin.[9–11,14,15] The block was then mounted to a microtome and serial sectioned at 3.0-μm thickness from the vitreous surface through the ONH into the retrolaminar orbital optic nerve. After each section was taken, the block surface was stained with a 1:1 (vol/vol) mixture of Ponceau S and acid fuchsin stains, then imaged at a resolution of 2.5×2.5 μm per pixel. The serial section images for each ONH were aligned in the anterior-to-posterior direction and stacked into a 3-D reconstruction of the ONH and peripapillary scleral connective tissue.

3-D Delineation of ONH and Peripapillary Scleral Landmarks

In each radial section image, the delineator marked seven structures and six pairs of neural canal landmarks (see Appendix Figs. A1, A2).[9–11] Three experienced delineators performed all the marking in this study. Both eyes of each animal were marked by one of them. The delineators were not masked to the IOP status of each eye; however, they were effectively unaware of the IOP status, because the delineation software did not contain that information. On completion of the delineation, the marks were checked for accuracy by two experienced observers (HY, CFB).

Clinical Alignment of 3-D ONH Reconstructions

For each ONH, a reconstruction of the central retinal vessels was used to clinically co-localize the 3-D reconstruction to a clinical photograph by using a qualitative match of the ONH and retinal vessels.[9–11,14,15,29]

TABLE 2. Overall Data for Each Monkey

Parameters	Monkey 1 N10	Monkey 1 ΔEEG*	Monkey 2 N10	Monkey 2 ΔEEG	Monkey 3 N10	Monkey 3 ΔEEG	Monkey 4 N10	Monkey 4 ΔEEG	Monkey 5 N10	Monkey 5 ΔEEG	Monkey 6 N10	Monkey 6 ΔEEG	Monkey 7 N10	Monkey 7 ΔEEG	Monkey 8 N10	Monkey 8 ΔEEG	Monkey 9 N10	Monkey 9 ΔEEG	PID*max*
Neural canal architecture, μm																			
NCO offset	629	13	648	12	565	37	590	2	615	21	516	**96**	579	**39**	NA	NA	728	−12	9
ASCO offset	729	57	755	17	607	14	648	11	712	1	617	**50**	724	71	671	**44**	785	23	16
ALI offset	783	4	779	19	608	19	649	11	736	4	619	**71**	726	**70**	669	**48**	787	22	16
PLI offset	974	14	861	20	672	**70**	721	**39**	836	**54**	688	**139**	904	**99**	778	**87**	852	**62**	18
PSCO offset	999	11	868	−19	736	**31**	743	**19**	861	**30**	736	**73**	940	**85**	820	**43**	880	20	22
ASAS offset	1162	−32	1046	−28	824	**33**	831	**39**	993	**74**	861	**98**	1038	**98**	914	**41**	978	−6	18
ASCO depth	38	2	34	−15	93	**−35**	29	4	53	2	24	−1	22	7	62	**−18**	11	1	15
ALI depth	50	−4	62	−13	96	**−35**	38	**18**	64	**14**	73	3	22	7	62	−7	44	**49**	20
PLI depth	113	−10	162	**18**	191	**−38**	166	**39**	145	**14**	165	**15**	86	−5	171	**−26**	163	**71**	20
PSCO depth	116	−7	183	−12	216	**−55**	181	**25**	153	7	185	**−26**	104	−9	200	**−58**	182	**40**	27
ASAS depth	131	**−39**	199	−5	219	**−63**	185	9	146	**−36**	190	**−68**	125	**−25**	200	**−88**	190	**−48**	25
ONH connective tissue, μm																			
Lamina cribrosa position	−113	**−29**	−109	**−45**	−126	**−61**	−111	**−97**	−105	**−79**	−114	**−68**	−102	**−118**	−106	**−117**	−97	**−184**	16
Peripapillary scleral position	0	4	−26	44	−71	**59**	−14	3	−37	35	−23	**39**	45	**21**	−43	77	NA	NA	16
Lamina cribrosa thickness	87	**30**	144	**52**	122	**−9**	128	**23**	83	**26**	140	**29**	103	**61**	139	**20**	136	**55**	18
Sclera plange thickness	NA	NA	73	8	103	−4	76	1	60	8	115	−8	69	7	92	**24**	NA	NA	14
Peripapillary scleral thickness	116	**−19**	156	**59**	138	**16**	126	**−32**	113	1	158	0	136	−4	146	−1	NA	NA	5
ONH laminar cupping																			
Post-NCO total prelaminar volume†‡	0.196	36%§	0.244	55%§	0.144	62%§	0.159	77%§	0.160	119%§	0.158	127%§	0.231	133%§	0.143	169%§	0.215	188%§	28.4%

Bold data denote significant difference ($P < 0.05$) by ANOVA. Shaded data denote that the between-eye difference achieved statistical significance and exceeded the PIDmax.
* Difference between EEG eye and normal eye.
† Statistical analysis is not applicable for this parameter.
‡ Percentage differences between EEG and normal eyes for this parameter were reported. The monkey order was determined by the magnitude of the change in this parameter.
§ Data exceeded PIDmax only.

Neural Canal Opening Reference Plane and Quantification

For each 3-D ONH reconstruction (see Appendix Figs. A2, A3), a plane satisfying a least-squares error restraint was fitted to the 80 NCO points,[9–11,14,15,30] creating a neural canal opening (NCO) reference plane (see Appendix Fig. A2C).[9,30] All NCO points were projected onto the fitted plane, an ellipse was fitted (NCO ellipse), and its centroid (NCO centroid) was used as the center point for most of the following measurements: NCO major diameter, NCO minor diameter, NCO area, neural canal depth and offset, laminar position, laminar thickness, peripapillary scleral position and thickness, scleral flange thickness, and post-NCO total prelaminar volume (PNCOTPV).

Statistical Analyses

A factorial analysis of variance (ANOVA) was performed to assess the effects of region (see Appendix Fig. A3) and treatment (N 10 vs. EEG 10, N10 vs. EEG 30, or N 10 vs. EEG 45) on the following parameters: neural canal depth and offset, laminar position and thickness, scleral flange thickness, and peripapillary scleral position and thickness, both overall and between the eyes of each animal. In this analysis, statistically significant differences between regions, treatments, and region-by-treatment interactions were found with an overall significance *F*-test followed by *t*-tests, with *P* values corrected for multiple comparisons.[31] In each animal, EPIDmax parameter differences in the EEG eye were those statistically significant differences that exceeded the maximum physiologic intereye difference (PID maximum) in the six bilaterally normal monkeys reported elsewhere.[14,15]

To assess for a treatment effect on axial length, we used a separate ANOVA to compare the baseline and axial length data before death of both eyes of each animal, followed by the Tukey honestly significant difference test between means.

Commercial software (MedCalc Software Bvba, Mariakerke, Belgium) was used to seek correlations between selected features of the normal eye anatomy that had been shown to be biomechanically important (Yang H, et al. *IOVS* 2009;50:ARVO E-Abstract 4890)[32–34] and a subset of the output parameters that demonstrated the most consistent change in the nine EEG eyes. Because we were deliberate in the number of, and logic for, the correlations we explored, we did not attempt to correct our *P* value for multiple comparisons ($P < 0.05$; Fig. 5).

To assess the magnitude of experiment-wide treatment effects and hypercompliance in the nine EEG eyes compared with previously reported normal eye data,[14] we performed a repeated-measures ANOVA, followed by adjusted *t*-tests on the differences of least square means. The 95% confidence intervals (95% CIs) for differences between the two groups of eyes in the following treatment groups were derived from their estimated mean values, as described in Appendix Table A2: (1) bilaterally normal eye differences, (2) normal eye compliance, (3) EEG eye permanent deformation, (4) EEG eye permanent plus EEG acute deformation, and (5) EEG eye compliance.

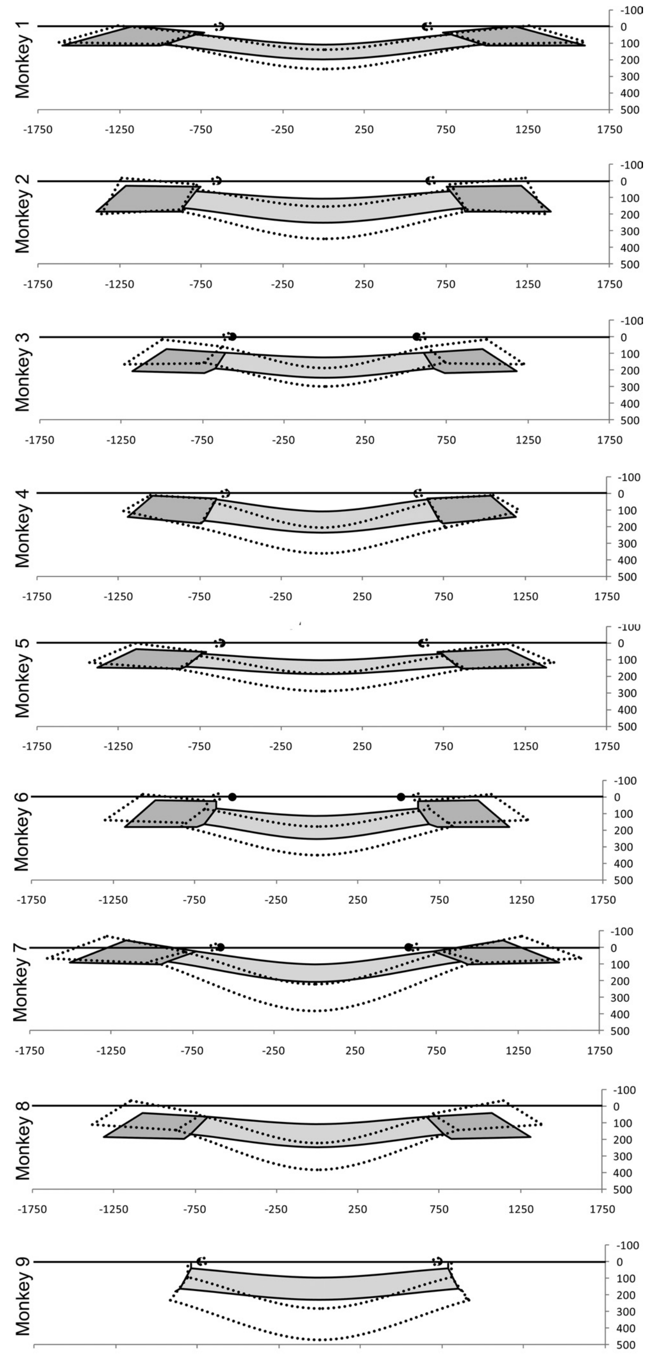

Figure 3. The overall data (in micrometers) for the normal (*shaded areas*) and EEG (*dotted lines*) ONH of each monkey as reported in Table 2. Qualitative differences between the nine normal eyes include laminar surface curvature (relatively flat, monkeys 2, 3, 5, and 6; relatively curved, monkeys 4 and 7). Laminar and peripapillary scleral thickness (relatively thin, monkeys 1 and 5; relatively thick, monkeys 2, 4, 6, 8, and 9); and NCO size and obliqueness (small and less oblique, monkeys 3 and 4; large and more oblique, monkeys 1, 5, and 7). In the nine EEG eyes, substantial neural canal expansion was present in four monkeys (3, 6, 7, and 8). Posterior LC deformation ranged from minimal (monkey 1) to substantial and was accompanied by minimal to substantial thickening in all EEG eyes except 1 (monkey 3). Marked posterior bowing of the peripapillary scleral (leaving it more anterior to its normal position) was present in six monkeys (2, 3, 5, 6, 7, and 8; data in monkey 9 were not available).

Results

Descriptive Data

Descriptive data are reported in Table 1 and Figures 1 and 2. When baseline and measurements obtained just before death were compared, the overall significant increase ($P < 0.0001$) in the axial length occurred in the EEG eyes (axial length immediately before death, 20.78 mm vs. baseline axial length, 20.19 mm), whereas no statistically significant changes in axial length were noted in the nine contralateral normal eyes. Individually, small but statistically significant increases in axial length (0.21–0.44 mm) were noted in five of the nine EEG eyes, whereas larger significant increases of 0.91 mm (monkey 2) and 1.7 mm (monkey 9) were noted in two of the EEG eyes.

Experiment-wide Analysis

Data for experiment-wide treatment effects are reported in Appendix Table A2. For most parameters, because of the magnitude of fixed deformation present in the EEG 10 eyes, no additional (or acute) deformation could be detected in the EEG 30/45 eyes.

Range of Deformation in the EEG 10 Compared with the EEG 30/45 Eyes

To test the hypothesis that a subset of EEG 30/45 eyes would demonstrate hypercompliance that would not be of a magnitude to drive the overall analysis, we recorded the individual EEG eye data reported in Table 2. The monkey number in this table (and throughout the study) reflects the least (monkey 1) through the most (monkey 9) overall connective tissue deformation, as characterized by the volumetric parameter PNCOTPV (Appendix Fig. A2G). For qualitative comparison, schematic plots of the overall data in Table 2 are presented for each animal in Figure 3.

The range of permanent deformation in the three EEG 10 eyes is compared to the range of total deformation (permanent plus acute) in the six EEG 30/45 eyes in Table 3. For most of the parameters, the maximum deformation in the six EEG 30/45 eyes far exceeded the maximum deformation in the three EEG 10 eyes. Thus, even if we assume that the maximum amount of deformation present in the three EEG 10 eyes was present in every EEG 30/45 eye before acute IOP elevation, depending on the parameter, we must take into account that at least two of the EEG 30/45 eyes (monkeys 8 and 9) demonstrated ONH connective tissue hypercompliance relative to the experiment-wide estimates of normal compliance reported in Appendix Table A2. Furthermore, if we assume that the minimum amount of permanent deformation was present in every EEG 30/45 eye before acute IOP elevation, the number of eyes demonstrating hypercompliance is even greater.

Characterization of Connective Tissue Deformation in the 9 EEG Eyes without Regard for the Level of IOP at the Time of Fixation

In the overall data in Table 2, EPIDmax expansion in PNCOTPV ranged from 36% in monkey 1 to 188% in monkey 9. Evidence of overall EPIDmax neural canal radial expansion (increase in neural canal offset) was present in seven monkeys and was most consistently present at the level of posterior laminar insertion. Evidence for overall neural canal depth change was not consistent in direction. A relative anteriorization of the ASAS (anteriormost aspect of the subarachnoid space) depth relative to the NCO was present in seven monkeys. Overall EPIDmax posterior laminar deformation was present in all nine monkeys, and laminar thickening was present in eight of nine. Overall EPIDmax peripapillary scleral bowing, which refers to outward deformation of the immediate peripapillary sclera relative to the more peripheral posterior sclera, manifesting as an EPIDmax increase in the peripapillary and posterior scleral position relative to the NCO reference plane, was present in six of the eight animals in which it could be measured. These overall results are plotted schematically in Figure 3. In these plots, qualitative differences between the nine normal eyes, including laminar surface curvature, laminar and peripapillary thickness, and neural canal size and obliqueness, can be appreciated.

Table 3. Actual Range of Deformations in EEG10 and EEG 30/45 Eyes

Parameters	Actual Range of Permanent Deformation in EEG10 Eyes*†		Actual Range of Total Deformation (Permanent Plus Acute) in EEG30/45 Eyes†‡§	
	Min	Max	Min	Max
Neural canal architecture, μm				
NCO offset	2	39	−12	96
ASCO offset	1	71	14	57
ALI offset	4	70	4	71
PLI offset	39	99	14	139
PSCO offset	19	85	−19	73
ASAS offset	39	98	−32	98
ASCO depth	2	7	2	−35
ALI depth	7	18	−35	49
PLI depth	−5	39	−38	71
PSCO depth	−9	25	40	−58
ASAS depth	9	−36	−5	−88
ONH connective tissue, μm				
Lamina cribrosa position	−79	−118	−29	−184
Peripapillary sclera position	3	35	4	77
Lamina cribrosa thickness	23	61	−9	55
Flange thickness	1	8	−8	24
Peripapillary sclera thickness	1	−32	−19	59
ONH laminar cupping, mm^3				
Post-NCO total prelaminar volume	77%	133%	36%	188%

The maximum and minimum values are listed without considering the direction of the deformation (only the magnitude of the deformation).

* The actual range of permanent deformation the three EEG10 eyes (compared with the contralateral normal eyes) as reported in Table 2.

† The fact that the full range of total deformation in the EEG30/45 eyes (right column) far exceeds the range of the permanent deformation (left column) suggests that at least a subset of the EEG30/45 eyes demonstrate hypercompliant deformation of their ONH connective tissues in response to acute IOP elevation at the time of death.

‡ The actual range of total deformation (permanent plus acute) in the six EEG 30/45 eyes compared with the contralateral normal eyes, as reported in Table 2.

§ The fact that the total deformation ranges in EEG 30/45 eyes pass through 0 for most parameters suggests only that the direction of both fixed and acute deformations in these eyes is eye specific and complicated.

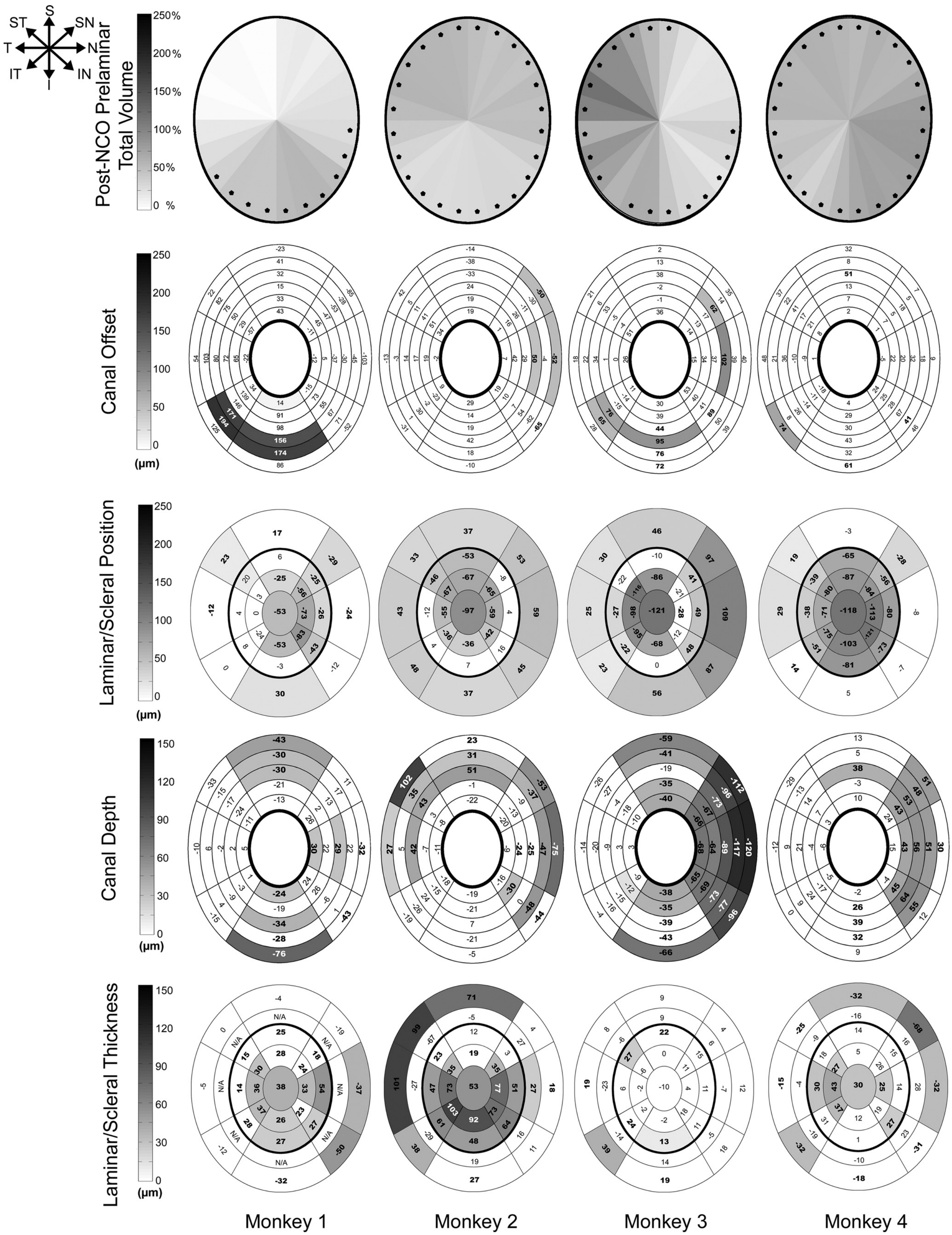
S
SN
N
IN
I
IT
T
ST
Post-NCO Prelaminar Total Volume
250%
200%
150%
100%
50%
0 %
Canal Offset
250
200
150
100
50
0
(µm)
Laminar/Scleral Position
250
200
150
100
50
0
(µm)
Canal Depth
150
120
90
60
30
0
(µm)
Laminar/Scleral Thickness
150
120
90
60
30
0
(µm)
Monkey 1
Monkey 2
Monkey 3
Monkey 4

FIGURE 4.

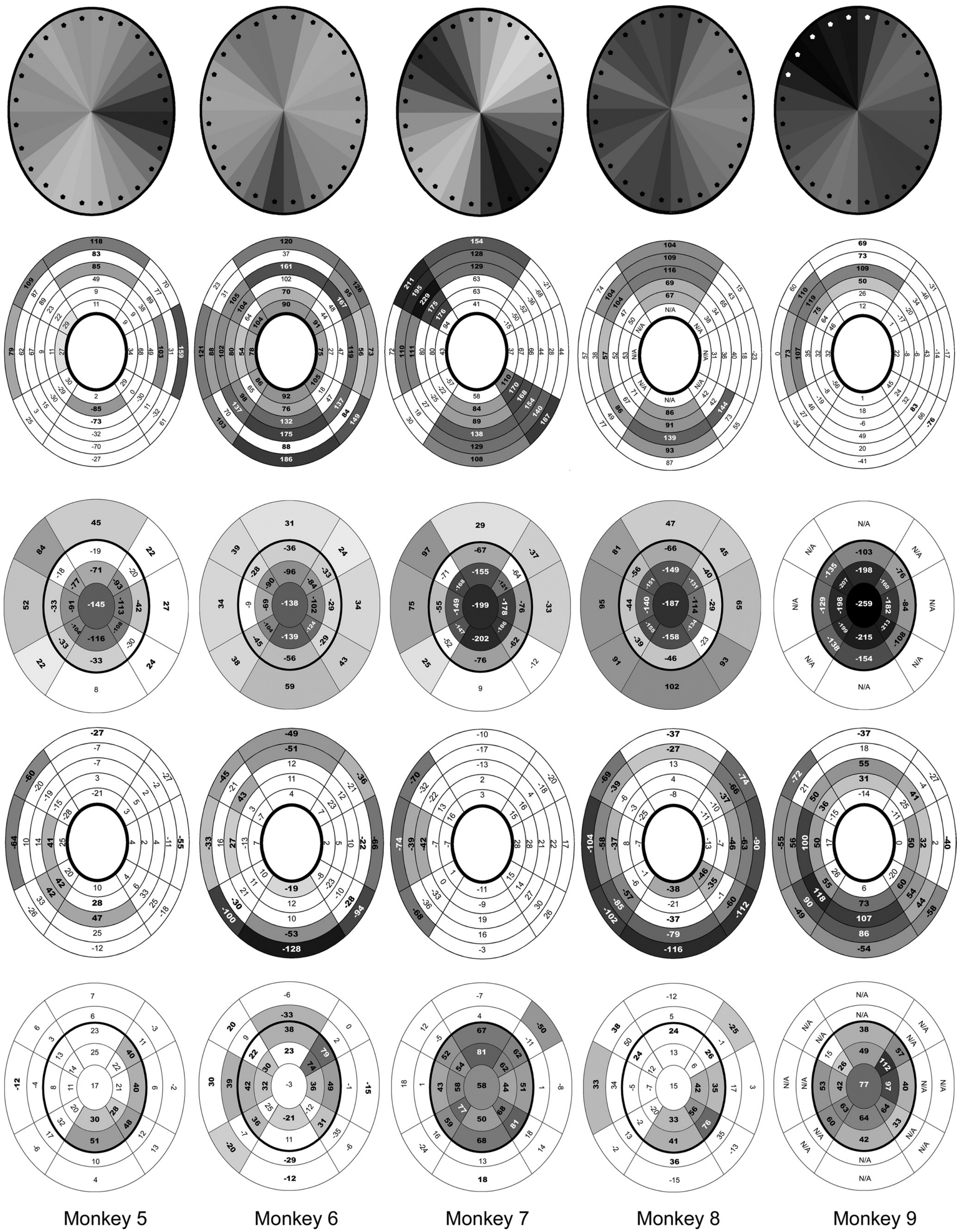

FIGURE 4. (*Continued*)

Statistically significant and EPIDmax regional differences between the EEG and normal eye of each monkey are reported for each parameter in Figure 4. Overall, there was a tendency toward segmental alteration in either the inferior nasal or superior temporal quadrants, with eventual co-localization of neural canal expansion, posterior laminar deformation, and posterior (outward) bowing of the peripapillary sclera in these two quadrants (Fig. 4; monkeys 5–9, top three rows).

In all nine EEG eyes, regional laminar thickening appeared to accompany the process of ONH and peripapillary position change from its onset and becomes generally more pronounced in magnitude and extent. It is important to note that there were no regions of EPIDmax laminar thinning in any of the nine EEG eyes and laminar thickness changes did not appear to precede laminar and or peripapillary scleral position changes in a single EEG eye. However, regional alterations in peripapillary scleral thickness were not substantial, consistent, or clearly progressive through this early stage of damage (i.e., monkeys 6, 7, and 8 did not have more pronounced changes compared with monkeys 1, 2, and 3). Finally, regional alterations in neural canal wall architecture (thinning or axial compression in six of nine monkeys and thickening or axial elongation in three of nine monkeys) were present in all EEG eyes. These changes, while substantial in some eyes, were not consistently more pronounced in the eyes with the greatest position changes (monkeys 5–9).

Correlations between EEG Eye Deformations, Normal Eye Anatomy, and IOP Insult by Single Linear Regressions

Among the 24 selected correlations we explored (see the Methods section), CSLT-detected EEG eye ONH surface change correlated positively with EEG eye cumulative IOP insult (Fig. 5; $P < 0.05$). EEG eye axial length increase correlated positively with maximum IOP insult ($P < 0.05$). EEG eye laminar thickness change positively correlated to normal eye anterior scleral canal opening (ASCO) size ($P < 0.05$). Finally, EEG eye PNCOTPV change, and laminar position and thickness change correlated with normal eye laminar position ($P < 0.05$), with a shallower laminar position in the normal eye (relative to NCO reference plane) predicting greater change in these three EEG eye parameters.

Discussion

The principal goals of this study were to retest the hypothesis that the monkey ONH connective tissues are altered by early glaucomatous damage in such a way that they become hypercompliant and to expand our initial 3-D characterization of early glaucomatous connective tissue deformation to a larger group of EEG eyes without regard for the level of IOP at the time of fixation.

The principal findings of this report are as follows. First, although the presence of overall ONH connective tissue hypercompliance in the 30/45 eyes could not be detected when the eyes were considered together, the presence of hypercompliant deformation is suggested in the individual eye data of a subset of the 30/45 eyes. Second, cupping in monkey EEG that occurs in the setting of modest to moderate chronic IOP elevations is defined by an expansion in PNCOTPV, which is due to co-localized posterior laminar deformation and neural canal expansion that is at maximum in the superior temporal and/or inferior–nasal quadrants. Third, posterior laminar deformation and neural canal wall expansion are accompanied by laminar thickening, axial elongation, and posterior (outward) peripapillary scleral bowing in most of the eyes.

Previous studies have demonstrated hypercompliance of the ONH surface[1] and lamina[12] early in the optic neuropathy of experimental glaucoma in young adult monkey eyes. Several factors probably contributed to our inability to detect overall hypercompliance in this EEG 30/45 group. First, our methods did not allow us to longitudinally quantify the fixed and acute portions of deformation in each EEG 30/45 eye before or after death. Second, the three EEG 10/10 animals (the very first EEG animals we reconstructed by 3-D histomorphometry)[9–11] were most likely killed at a later stage of connective tissue damage (that included more fixed deformation) than were the EEG 30/45 animals. Third, the timing of the hypercompliant stage of damage may be eye specific and occur at a later stage of experimental glaucoma damage or at higher levels of IOP insult than we studied in most of the EEG 30/45 eyes. Spectral-domain optical coherence tomography (SD-OCT)-determination of laminar position relative to the NCO[9,30,35] will allow longitudinal in vivo laminar compliance testing[36] (Burgoyne CF, et al. *IOVS* 2008;49:ARVO E-Abstract 3655) and primary detection of permanent and/or hypercompliant laminar deformation in monkey eyes with experimental ocular hypertension.

When the nine EEG eyes of this report are considered without regard to the IOP at the time of kill, a range of early glaucomatous ONH connective tissue deformation is present. Although the acute IOP elevation that preceded death may have influenced the postmortem deformation in a subset of eyes, at least three additional factors are likely to be important in explaining this variation: differences in the stage of EEG; differences in the magnitude, duration, and fluctuation of chronic IOP elevation; and differences in eye-specific ONH connective tissue geometry and material properties.

Although it was our intention to kill the nine EEG monkeys at an identical clinical endpoint (the onset of CSLT ONH surface change as defined by our parameter MPD), our infrastructure for real-time ONH surface change detection by CSLT was not operational at the time these animals were studied. It is obvious in retrospect that the nine EEG eyes represent a range of CSLT-defined EEG, with some eyes clearly beyond

Figure 4. Regional parameter difference maps for the EEG eyes by monkey (*columns*) and parameter (*rows*). These maps demonstrate regional co-localization of statistically significant (*bold data*; $P < 0.05$; ANOVA) and EPIDmax (*shaded*) differences in the EEG eye of each animal. Data are the magnitude of change in the EEG eye relative to its contralateral normal control. Positive and negative values in the shaded regions are defined for each parameter as follows: canal offset, radial expansion/radial contraction of the canal; LC position, anterior (inward) movement/posterior (outward) of the anterior laminar surface; PNCOTPV, expansion/contraction of the space beneath the NCO reference plane, above the lamina and in the neural canal wall (For PNCOTPV, the regional differences that exceeded PID maximum differences are marked by *dots*.); positive peripapillary scleral position, anterior (inward) shift of the peripapillary sclera relative to the NCO reference plane, which most likely reflects posterior (outward) bowing of the peripapillary sclera and NCO reference plane (together) relative to the more peripheral sclera; canal depth, axial thickening/axial thinning of the canal; LC thickness, thickening/thinning; and peripapillary scleral thickness, thickening/thinning of the peripapillary sclera; All data are plotted in right-eye configuration. S, superior; SN, superonasal; N, nasal; IN, inferonasal; I, inferior; IT, inferotemporal; T, temporal; ST, superotemporal. See Appendix Figure A3 for a detailed description of regionalization.

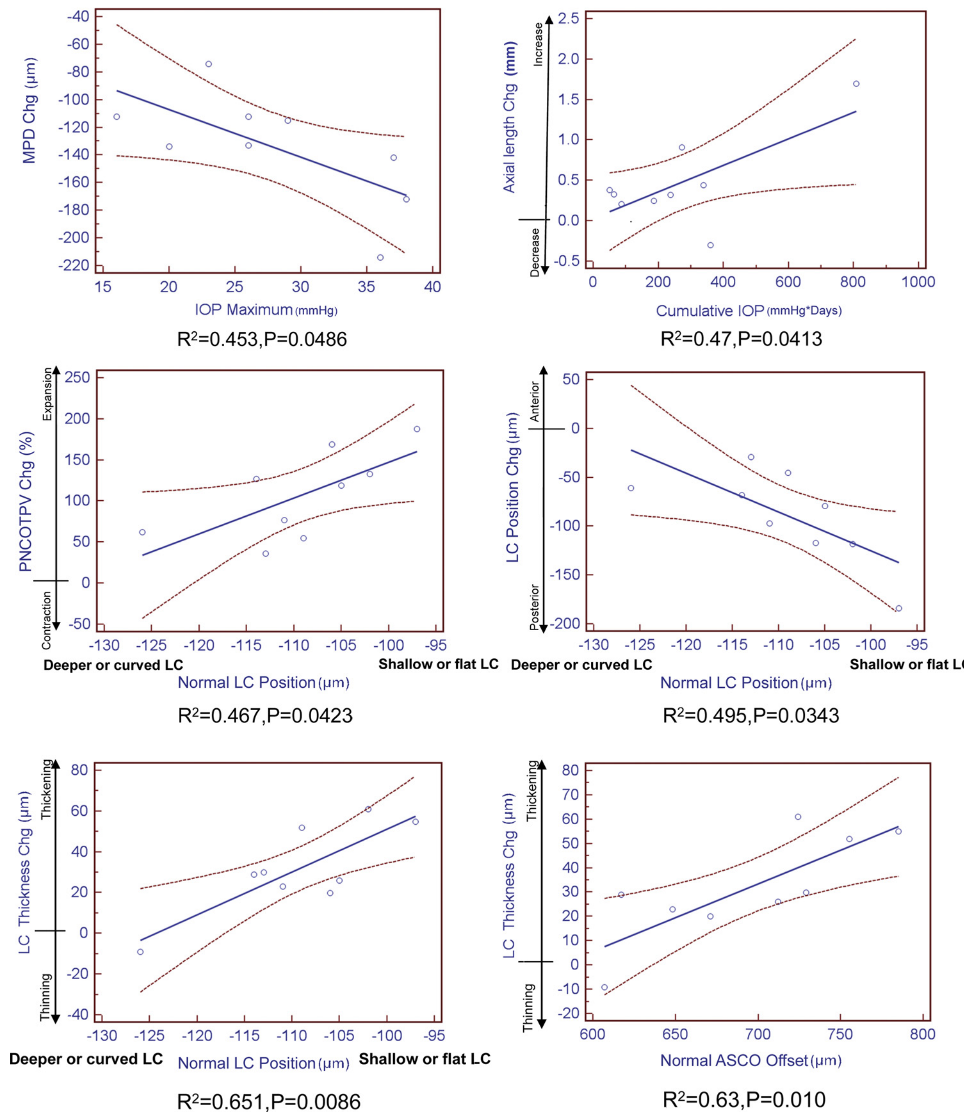

FIGURE 5. Correlation plots. Only the significant correlations between the input parameters IOP maximum, cumulative IOP insult, normal eye ASCO offset, normal eye scleral thickness, normal-eye LC thickness and position, and the EEG eye output parameters PNCOTPV percentage change versus the normal eye, LC thickness change versus the normal eye, MPD change versus its baseline and axial length change versus its baseline are shown. All measurements except axial length change are in micrometers. *Blue slopes*: fitted linear regression; *dotted brown curves*: the 95% CI of the regression; *blue circles*: individual values.

early surface alterations, as characterized by TCA analysis (Fig. 2). Although axon counts are pending in five of the six EEG 30/45 eyes, we have reported a similar range of orbital optic nerve axon loss in a subset of the nine EEG eyes (30%, 19%, and 16% in monkeys 4, 5, and 7 respectively,[11] and 16% in monkey 1; data not shown) (Burgoyne CF, et al. *IOVS* 2005;46:ARVO E-Abstract 2372).

Although telemetric monitoring of IOP in our animals is under development (Downs JC, et al. *IOVS* 2008;49:ARVO E-Abstract 2043; Downs JC, et al. *IOVS* 2009;50:ARVO E-Abstract 2842), the cumulative IOP and maximum postlaser IOP data we report are based on weekly to biweekly IOP measurements. In this study, cumulative IOP insult correlated with ONH surface change (MPD change), and maximum postlaser IOP correlated with axial length change, but neither demonstrated a correlation with our principal measures of ONH connective tissue deformation. In fact, animals 7 and 8 demonstrated the second and third greatest magnitude of ONH connective tissue deformation, yet each was exposed to relatively low (or the lowest) levels of cumulative IOP and maximum postlaser IOP elevation.

ONH connective tissue geometry and material properties were probably different among the nine EEG eyes before the onset of IOP elevation, and these differences may strongly influence their susceptibility to IOP-related deformation and damage. That the geometries of the EEG eyes (when normal) were different from one another is to be expected and can be deduced from the postmortem geometry differences among the nine normal eyes (Table 2, Fig. 3).

The degree to which the constituent material properties of the lamina and peripapillary and posterior sclera were different among the nine normal eyes will be estimated in engineering finite element models of each normal eye that are currently under construction in our collaborative laboratory. In the future, in vivo baseline and predeath estimates of ONH connective tissue architecture and material properties for each studied eye will be produced from longitudinally performed SD-OCT ONH connective tissue compliance testing. These estimates, along with a telemetric characterization of IOP insult, will allow us to more powerfully assess how IOP insult, ONH connective tissue architecture, and ONH connective tissue material properties each contribute to the EEG ONH connective tissue alterations that develop in the individual monkey eye.

Of note, even with only nine animals studied, some features of the normal eye anatomy did correlate with specific ONH connective tissue outcome measures in the EEG eyes. Normal eye laminar position correlated with expansion of PNCOTPV, laminar posterior deformation (a component of PNCOTPV), and laminar thickness change. Normal eye ASCO offset (a measure of anterior scleral canal size) separately correlated with laminar thickness change. Previous parametric finite element modeling studies have demonstrated that normal monkey ONH connective tissue deformations after acute IOP elevations are sensitive to geometry and material properties.[33,37–40] More recent studies[32,34] (Yang H, et al. *IOVS* 2009;50:ARVO E-Abstract 4890) have established that LC position in the canal is an important determinant of laminar behavior after acute and chronic IOP elevations. In future multivariate analyses of more than 40 EEG monkeys, we will seek baseline predictors of IOP-induced ONH connective tissue deformation.

Expansion in PNCOTPV that is the result of a combination of posterior deformation of the LC and scleral canal expansion was accompanied by LC thickening in all nine EEG eyes at least regionally. The relative co-localization of these phenomenon is schematically depicted in Figure 6. The presence of PNCOTPV expansion in all nine EEG eyes confirms that a primary laminar or connective tissue component of cupping underlies the optic neuropathy of early experimental monkey glaucoma.[10] The presence of at least regional laminar thickening in all nine EEG eyes, confirms that, in response to IOP elevation, IOP-induced deformation, or both, the lamina is being actively remodeled in a manner that may involve retrolaminar septal recruitment.[19]

We observed overall posterior (outward) bowing of the peripapillary sclera in six of the nine animals. Regional peripapillary scleral bowing (but no increase in axial length) was present in two of the three remaining EEG eyes (scleral data were not available for monkey 9). These data extend our previous findings in the three EEG 10 eyes[10] to the 30/45 eyes. The fact that the experiment-wide estimate of EEG eye compliance in the 30/45 eyes (27–38 μm) exceeds that of six N 30/45 eyes (13–17 μm) from a previous report, strongly suggests that the peripapillary sclera not only is permanently deformed, but also is hypercompliant at this stage of the neuropathy (see Appendix Table A2). Transitory scleral hypercompliance is present in the scleral material property testing data of a separate group of EEG eyes (Girard MJ, et al. *IOVS* 2009;50:ARVO E-Abstract 5217). The cellular and extracellular matrix changes that underlie these alterations remain to be determined.

The six EEG eyes that demonstrated overall peripapillary scleral bowing (monkeys 2, 3, 5, 6, 7, and 8) also demonstrated significant increases in axial length (measured in vivo near the fovea, but not precisely, because the animal does not fixate on a target during measurement). These data suggest that chronic IOP elevation induces chronic globe expansion[41–43] plus a separate and additional outward bowing of the peripapillary sclera. Or, it may be the case that the outward bowing of the peripapillary sclera extends into the fovea and is the cause for the measured increase in axial length. Diffuse expansion of the globe has been shown to occur after acute and chronic IOP elevation in a variety of species.[41–46] We have reported axial length increases in a subset of monkey EEG eyes.[12]

Several groups studied the relationship between axial length and laminar and scleral thickness in normal and human glaucomatous eyes. Nemeth[42] found a strong inverse correlation between axial length and posterior scleral thickness in glaucomatous eyes. Jonas and Holbach[47] found that LC thickness in normal eyes also correlates inversely with axial length[47] and that the lamina is markedly thinner in non–highly myopic eyes with advanced glaucomatous optic nerve damage than in normal eyes.[48] In a more recent study, Ren et al.[43] demonstrated that axially elongated glaucomatous eyes have a thinner lamina and sclera (just outside the optic nerve meninges) than do normal eyes and glaucomatous eyes with normal axial length. However, in their study, scleral thickness of the glaucomatous eye with normal axial length did not differ from normal eyes. Finally, Norman et al.[41] reported that ostensibly glaucomatous eyes tended to be axially elongated and had thinner posterior sclera than did normal eyes.

In the present study, we did not find consistent thinning of the peripapillary sclera at this early stage of glaucomatous damage. However, we have reported thinning of the posterior sclera (away from the ONH) in a separate group of monkeys with a similar stage of damage,[49] although it is still unknown whether thinning of the sclera increases the risk of IOP-induced glaucomatous damage.[33,38] The magnitude and frequency of axial length elongation in monkey EEG and its relationship to peripapillary scleral bowing and thickness alterations will be the subject of a future report.

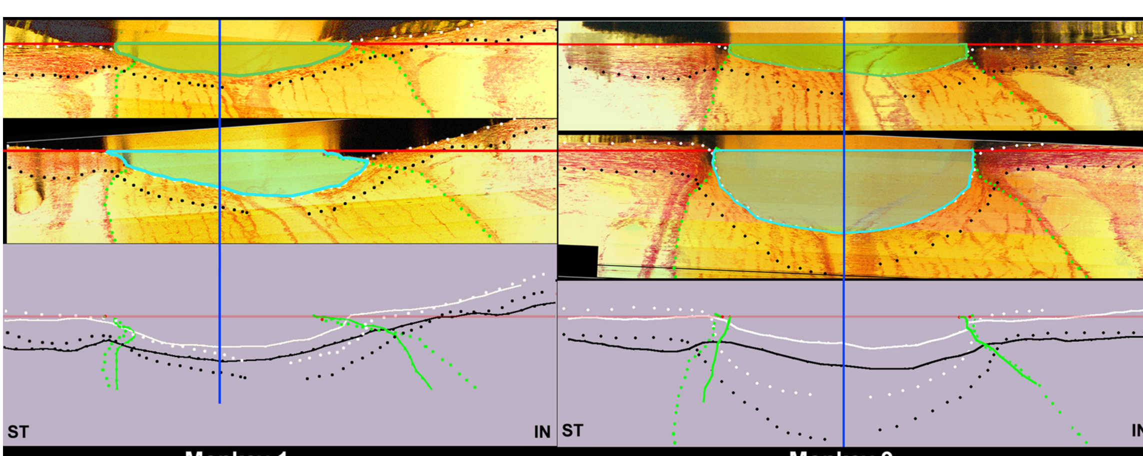

FIGURE 6. The range of PNCOTPV expansion between monkey 1 (minimum PNCOTPV expansion) and monkey 9 (maximum PNCOTPV expansion). The following landmarks are delineated in representative superior temporal (ST) to inferior nasal (IN) digital sections from the normal (*top*) and EEG (*middle*) eye of both animals: anterior scleral/laminar surface (*white dots*), posterior scleral/laminar surface (*black dots*), neural boundary (*green dots*), NCO reference plane (*red line*), and NCO centroid (*vertical blue line*). *Bottom*: delineated points for the normal (*solid lines*) and EEG eye of each eye are overlaid relative to the NCO centroid. For each animal, PNCOTPV is outlined in both the normal (*top*, *dark green*) and EEG (*middle*, *light blue*) eye for qualitative comparison. The overlaid delineations for both eyes of each animal (*bottom*) suggest that regional PNCOTPV expansion is due to posterior laminar deformation and neural canal expansion from its onset (monkey 1) and that these two phenomena continue through the more advanced stages of connective tissue deformation and remodeling (monkey 9). These phenomena are accompanied by regional laminar thickening and outward bowing of the peripapillary sclera in both of these animals and most of the 9 EEG eyes.

There is a tendency for either inferonasal and/or superotemporal co-localization of posterior laminar deformation and neural canal expansion in the eyes with the least connective tissue deformation (monkeys 1–4, Fig. 4), whereas the same two quadrants are together involved in the eyes with the greatest deformation (monkeys 5–9, Fig. 4). These postmortem data suggest that two important phenomena may be present in a separate group of EEG eyes that are currently longitudinally being observed with SD-OCT imaging technique[30,35,50–54]: first, that most eyes will manifest early maximum connective tissue deformation in one of these two quadrants; and second, that the detection of early segmental connective tissue deformation will predict an axis of subsequent maximum connective tissue deformation, along an axis through the NCO centroid.

We acknowledge, however, that although the NCO centroid is a useful datum from which to reference measurements such as these, it is not a biological determinant of these effects.

We predict that there are biomechanical determinants[19] (Grimm J, et al. *IOVS* 2007;48:ARVO E-Abstract 3295; Grimm J, et al. *IOVS* 2010;51:ARVO E-Abstract 1776) for the phenomena we have described herein. Regional differences in LC connective tissue volume fraction, beam thickness, and laminar pore size—all determinants of load-bearing in the LC and acting in concert with the structural stiffness of the surrounding sclera—for both eyes of all nine EEG animals will be the subject of a future report. As these data become available and are complemented by longitudinal data, a more complete portrait of the relationship between acute IOP-related strain (and stress) and its longer term effect on LC deformation and remodeling will emerge.

We have discussed the limitations of our methods in great detail.[9–11,14,15] In the present study, we saw evidence of residual blood in the retinal and posterior ciliary circulation in the high IOP EEG eyes that suggests less than ideal fixative perfusion. Although all eyes remained at their set IOP for 60 minutes after perfusion to enhance fixation, it is possible that our data variably underestimate the magnitude of ONH connective tissue deformation in the high-IOP eyes.

Our measurements were made relative to an NCO reference plane.[9,30] Any collapse of the border tissue of Elschnig or compression of the choroid either from chronic or acute IOP elevation or from post-trephination tissue warping, could alter these points, leading to a posterior shift or tilt of the reference plane in the EEG eye. Such an artifact would induce anterior movement or tilting of the other structures relative to its contralateral normal eye. Close examination of the canal depth data in four monkeys, 1, 3, 6, and 8, showed regional compression of the distance (reduced ASCO depth) between the ASCO and the NCO reference plane. However, only monkey 3 demonstrated findings compatible with the tilt (less LC posterior deformation on the nasal than on the temporal side; see Fig. 4).

Our study included four rhesus and five cynomolgus monkeys (Table 1) which may confound our results. Although there may be species differences in monkey ONH architecture and material properties that influence their response to both chronic and acute IOP elevation,[12,13,55] we doubt that these differences affected the results in our study for the following reasons. First, there are no obvious differences between the normal eye measurements in the two species (Table 2). Second, there was no clear separation of the two species when we tried to order overall deformations in the EEG eye (Table 2, Fig. 4).

Finally, because of the fundamental differences in the geometry and material properties of the ONH and peripapillary sclera between monkeys and humans, our findings in monkeys may have limited application to the human eye. Although human sclera is two to four times thicker[41,49,55–59] than monkey sclera, a direct comparison of scleral material properties using the same testing apparatus and modeling strategy has not yet been performed. The human LC is also thicker than that of the monkey (119–463 μm in humans[47,60–62] vs. 117–210 μm in monkeys[10,12,14,15]), although its material properties in both species are at present unknown.

Our finding of ONH connective tissue deformation that co-localized to the inferonasal and/or superotemporal quadrants in these nine monkey eyes is different from those in human glaucoma in which early neuroretinal rim changes in the inferior and superior temporal quadrants are traditionally described.[63–66] Several concepts regarding this apparent difference are important to discuss. First, the early stage of damage we describe has never been studied in human eyes. Second, our report describes connective tissue rather than neuroretinal rim alterations. Third regional susceptibility in the monkey eye may be more individual-eye–specific or frankly different from the human eye because of differences in the regional pattern of LC beams[19,67,68] and pores[67–71]; the regional distribution of connective tissue material properties[59,72–78]; the spatial relationship between the exit of the central retinal vessel trunk on the LC surface[79,80]; and the regional distribution of the translaminar pressure gradient.[81–83]

In summary, our data suggest that at the onset of CSLT detected ONH surface change in monkeys exposed to chronic, unilateral, and modest to moderate experimental IOP elevations, at least a subset of eyes demonstrated ONH connective tissue hypercompliance. However, all the EEG eyes demonstrated posterior laminar deformation, neural canal expansion, LC thickening, and posterior (outward) bowing of the peripapillary sclera that became relatively co-localized to the inferior nasal and/or superior temporal quadrants. The implications of these connective tissue deformations on the blood supply and cell biology of the adjacent astrocytes, glia, and retinal ganglion cell axons,[84] and the ability to predict the location of their greatest magnitude from in vivo characterizations of ONH connective tissue architecture, are currently under study in our laboratory.

Acknowledgments

The authors thank Jonathon Grimm and Juan Reynaud for assistance with software for volumetric and thickness quantification; Galen Williams and Erica Dyrud for help with delineation; Pris Zhou and Anthony Bellezza, PhD, for directing animal testing; Joanne Couchman for assistance with manuscript preparation and submission; and Stuart Gardiner for statistical consultation.

References

1. Burgoyne CF, Quigley HA, Thompson HW, Vitale S, Varma R. Early changes in optic disc compliance and surface position in experimental glaucoma. *Ophthalmology.* 1995;102:1800–1809.
2. Derick RJ, Pasquale LR, Pease ME, Quigley HA. A clinical study of peripapillary crescents of the optic disc in chronic experimental glaucoma in monkey eyes. *Arch Ophthalmol.* 1994;112:846–850.
3. Gaasterland D, Tanishima T, Kuwabara T. Axoplasmic flow during chronic experimental glaucoma. 1. Light and electron microscopic studies of the monkey optic nervehead during development of glaucomatous cupping. *Invest Ophthalmol Vis Sci.* 1978;17:838–846.
4. Pederson JE, Gaasterland DE. Laser-induced primate glaucoma. I. progression of cupping. *Arch Ophthalmol.* 1984;102:1689–1692.
5. Dandona L, Hendrickson A, Quigley HA. Selective effects of experimental glaucoma on axonal transport by retinal ganglion cells to the dorsal lateral geniculate nucleus. *Invest Ophthalmol Vis Sci.* 1991;32:1593–1599.
6. Quigley HA, Sanchez RM, Dunkelberger GR, L'Hernault NL, Baginski TA. Chronic glaucoma selectively damages large optic nerve fibers. *Invest Ophthalmol Vis Sci.* 1987;28:913–920.

7. Hayreh SS, Pe'er J, Zimmerman MB. Morphologic changes in chronic high-pressure experimental glaucoma in rhesus monkeys. *J Glaucoma.* 1999;8:56–71.
8. Quigley HA, Hohman RM. Laser energy levels for trabecular meshwork damage in the primate eye. *Invest Ophthalmol Vis Sci.* 1983;24:1305–1307.
9. Downs JC, Yang H, Girkin C, et al. 3-D histomorphometry of the normal and early glaucomatous monkey optic nerve head: neural canal and subarachnoid space architecture. *Invest Ophthalmol Vis Sci.* 2007;48:3195–3208.
10. Yang H, Downs JC, Girkin C, et al. 3-D histomorphometry of the normal and early glaucomatous monkey optic nerve head: lamina cribrosa and peripapillary scleral position and thickness. *Invest Ophthalmol Vis Sci.* 2007;48:4597–4607.
11. Yang H, Downs JC, Bellezza AJ, Thompson H, Burgoyne CF. 3-D histomorphometry of the normal and early glaucomatous monkey optic nerve head: prelaminar neural tissues and cupping. *Invest Ophthalmol Vis Sci.* 2007;48:5068–5084.
12. Bellezza AJ, Rintalan CJ, Thompson HW, Downs JC, Hart RT, Burgoyne CF. Deformation of the lamina cribrosa and anterior scleral canal wall in early experimental glaucoma. *Invest Ophthalmol Vis Sci.* 2003;44:623–637.
13. Burgoyne CF, Downs JC, Bellezza AJ, Hart RT. Three-dimensional reconstruction of normal and early glaucoma monkey optic nerve head connective tissues. *Invest Ophthalmol Vis Sci.* 2004;45:4388–4399.
14. Yang H, Downs JC, Burgoyne CF. Physiologic intereye differences in monkey optic nerve head architecture and their relation to changes in early experimental glaucoma. *Invest Ophthalmol Vis Sci.* 2009;50:224–234.
15. Yang H, Downs JC, Sigal IA, Roberts MD, Thompson H, Burgoyne CF. Deformation of the normal monkey optic nerve head connective tissue after acute IOP elevation within 3-D histomorphometric reconstructions. *Invest Ophthalmol Vis Sci.* 2009;50:5785–5799.
16. Roberts MD, Sigal IA, Liang Y, Burgoyne CF, Downs JC. Changes in the biomechanical response of the optic nerve head in early experimental glaucoma. *Invest Ophthalmol Vis Sci.* 2010;51:5675–5684.
17. Roberts MD, Liang Y, Sigal IA, et al. Correlation between local stress and strain and lamina cribrosa connective tissue volume fraction in normal monkey eyes. *Invest Ophthalmol Vis Sci.* 2010;51:295–307.
18. Downs JC, Suh JK, Thomas KA, Bellezza AJ, Hart RT, Burgoyne CF. Viscoelastic material properties of the peripapillary sclera in normal and early-glaucoma monkey eyes. *Invest Ophthalmol Vis Sci.* 2005;46:540–546.
19. Roberts MD, Grau V, Grimm J, et al. Remodeling of the connective tissue microarchitecture of the lamina cribrosa in early experimental glaucoma. *Invest Ophthalmol Vis Sci.* 2009;50:681–690.
20. Bengtsson B, Heijl A. Diurnal IOP fluctuation: not an independent risk factor for glaucomatous visual field loss in high-risk ocular hypertension. *Graefes Arch Clin Exp Ophthalmol.* 2005;243:513–518.
21. Ren R, Jonas JB, Tian G, et al. Cerebrospinal fluid pressure in glaucoma: a prospective study. *Ophthalmology.* 2010;117:259–266.
22. Quigley HA, Addicks EM, Green WR, Maumenee AE. Optic nerve damage in human glaucoma. II. The site of injury and susceptibility to damage. *Arch Ophthalmol.* 1981;99:635–649.
23. Bergea B, Bodin L, Svedbergh B. Impact of intraocular pressure regulation on visual fields in open-angle glaucoma. *Ophthalmology.* 1999;106:997–1004;discussion 1004–1005.
24. Caprioli J, Coleman AL. Intraocular pressure fluctuation a risk factor for visual field progression at low intraocular pressures in the advanced glaucoma intervention study. *Ophthalmology.* 2008;115:1123–1129 e1123.
25. Medeiros FA, Weinreb RN, Zangwill LM, et al. Long-term intraocular pressure fluctuations and risk of conversion from ocular hypertension to glaucoma. *Ophthalmology.* 2008;115:934–940.
26. Quigley HA, Addicks EM. Chronic experimental glaucoma in primates. I. Production of elevated intraocular pressure by anterior chamber injection of autologous ghost red blood cells. *Invest Ophthalmol Vis Sci.* 1980;19:126–136.
27. Quigley HA, Addicks EM. Chronic experimental glaucoma in primates. II. Effect of extended intraocular pressure elevation on optic nerve head and axonal transport. *Invest Ophthalmol Vis Sci.* 1980;19:137–152.
28. Heickell AG, Bellezza AJ, Thompson HW, Burgoyne CF. Optic disc surface compliance testing using confocal scanning laser tomography in the normal monkey eye. *J Glaucoma.* 2001;10:369–382.
29. Strouthidis NG, Yang H, Downs JC, Burgoyne CF. Comparison of clinical and three-dimensional histomorphometric optic disc margin anatomy. *Invest Ophthalmol Vis Sci*. 2009;50:2165–2174.
30. Strouthidis NG, Yang H, Fortune B, Downs JC, Burgoyne CF. Detection of optic nerve head neural canal opening within histomorphometric and spectral domain optical coherence tomography data sets. *Invest Ophthalmol Vis Sci.* 2009;50:214–223.
31. Edwards D, Berry JJ. The efficiency of simulation-based multiple comparisons. *Biometrics.* 1987;43:913–928.
32. Yang H, Sigal IA, Roberts MD, Burgoyne CF, Downs JC. The influence of material properties and geometry on optic nerve head biomechanics. *ASME Summer Bioengineering Conference.* Lake Tahoe, CA: June 2009.
33. Sigal IA, Flanagan JG, Ethier CR. Factors influencing optic nerve head biomechanics. *Invest Ophthalmol Vis Sci.* 2005;46:4189–4199.
34. Sigal IA, Yang H, Roberts MD, Burgoyne CF, Downs JC. IOP-induced lamina cribrosa displacement and scleral canal expansion: an analysis of factor interactions using parameterized eye-specific models. *Invest Ophthalmol Vis Sci.* First published on September 29, 2010 as doi:iovs.10-5500[pii]10.1167/iovs.10-5500.
35. Strouthidis NG, Grimm J, Williams G, Cull G, Wilson DJ, Burgoyne CF. A comparison of optic nerve head morphology viewed by spectral domain optical coherence tomography and by serial histology. *Invest Ophthalmol Vis Sci.* 2010;51:1464–1474.
36. Fortune B, Yang H, Strouthidis NG, et al. The effect of acute intraocular pressure elevation on peripapillary retinal thickness, retinal nerve fiber layer thickness and retardance. *Invest Ophthalmol Vis Sci.* 2009;50:4719–4726.
37. Sigal IA, Flanagan JG, Tertinegg I, Ethier CR. Finite element modeling of optic nerve head biomechanics. *Invest Ophthalmol Vis Sci.* 2004;45:4378–4387.
38. Sigal IA. Interactions between geometry and mechanical properties on the optic nerve head. *Invest Ophthalmol Vis Sci.* 2009;50:2785–2795.
39. Sander EA, Downs JC, Hart RT, Burgoyne CF, Nauman EA. A cellular solid model of the lamina cribrosa: mechanical dependence on morphology. *J Biomech Eng.* 2006;128:879–889.
40. Bellezza AJ, Hart RT, Burgoyne CF. The optic nerve head as a biomechanical structure: initial finite element modeling. *Invest Ophthalmol Vis Sci.* 2000;41:2991–3000.
41. Norman RE, Flanagan JG, Rausch SM, et al. Dimensions of the human sclera: thickness measurement and regional changes with axial length. *Exp Eye Res.* 2010;90:277–284.
42. Nemeth J. The posterior coats of the eye in glaucoma: an echobiometric study. *Graefes Arch Clin Exp Ophthalmol.* 1990;228:33–35.
43. Ren R, Wang N, Li B, et al. Lamina cribrosa and peripapillary sclera histomorphometry in normal and advanced glaucomatous Chinese eyes with various axial length. *Invest Ophthalmol Vis Sci.* 2009;50:2175–2184.
44. Phillips JR, McBrien NA. Pressure-induced changes in axial eye length of chick and tree shrew: significance of myofibroblasts in the sclera. *Invest Ophthalmol Vis Sci.* 2004;45:758–763.
45. Leydolt C, Findl O, Drexler W. Effect of change in intraocular pressure on axial eye length and lens position. *Eye.* 2008;2:657–661.
46. Chen YF, Wang TH, Lin LL, Hung PT. Influence of axial length on visual field defects in primary open-angle glaucoma. *J Formos Med Assoc.* 1997;96:968–971.
47. Jonas JB, Holbach L. Central corneal thickness and thickness of the lamina cribrosa in human eyes. *Invest Ophthalmol Vis Sci.* 2005;46:1275–1279.
48. Jonas JB, Berenshtein E, Holbach L. Lamina cribrosa thickness and spatial relationships between intraocular space and cerebrospinal

fluid space in highly myopic eyes. *Invest Ophthalmol Vis Sci.* 2004;45:2660–2665.

49. Downs JC, Ensor ME, Bellezza AJ, Thompson HW, Hart RT, Burgoyne CF. Posterior scleral thickness in perfusion-fixed normal and early-glaucoma monkey eyes. *Invest Ophthalmol Vis Sci.* 2001;42: 3202–3208.
50. Zawadzki RJ, Choi SS, Fuller AR, Evans JW, Hamann B, Werner JS. Cellular resolution volumetric in vivo retinal imaging with adaptive optics-optical coherence tomography. *Opt Express.* 2009;17: 4084–4094.
51. Torti C, Povazay B, Hofer B, et al. Adaptive optics optical coherence tomography at 120,000 depth scans/s for non-invasive cellular phenotyping of the living human retina. *Opt Express.* 2009;17: 19382–19400.
52. Strouthidis NG, Yang H, Reynaud J, et al. Comparison of clinical and spectral domain optical coherence tomography optic disc margin anatomy. *Invest Ophthalmol Vis Sci.* 2009;50:4709–4718.
53. Kagemann L, Ishikawa H, Wollstein G, et al. Ultrahigh-resolution spectral domain optical coherence tomography imaging of the lamina cribrosa. *Ophthalmic Surg Lasers Imaging.* 2008;39:S126–S131.
54. Srinivasan VJ, Adler DC, Chen Y, et al. Ultrahigh-speed optical coherence tomography for three-dimensional and en face imaging of the retina and optic nerve head. *Invest Ophthalmol Vis Sci.* 2008;49:5103–5110.
55. Downs JC, Blidner RA, Bellezza AJ, Thompson HW, Hart RT, Burgoyne CF. Peripapillary scleral thickness in perfusion-fixed normal monkey eyes. *Invest Ophthalmol Vis Sci.* 2002;43:2229–2235.
56. Oliveira C, Tello C, Liebmann J, Ritch R. Central corneal thickness is not related to anterior scleral thickness or axial length. *J Glaucoma.* 2006;15:190–194.
57. Lam A, Sambursky RP, Maguire JI. Measurement of scleral thickness in uveal effusion syndrome. *Am J Ophthalmol.* 2005;140: 329–331.
58. Olsen TW, Aaberg SY, Geroski DH, Edelhauser HF. Human sclera: thickness and surface area. *Am J Ophthalmol.* 1998;125:237–241.
59. Girard MJ, Suh JKF, Bottlang M, Burgoyne CF, Downs JC. Scleral biomechanics in the aging monkey eye. *Invest Ophthalmol Vis Sci.* 2009;50:5226–5237.
60. Quigley HA, Hohman RM, Addicks EM, Massof RW, Green WR. Morphologic changes in the lamina cribrosa correlated with neural loss in open-angle glaucoma. *Am J Ophthalmol.* 1983;95:673–691.
61. Yan DB, Coloma FM, Metheetrairut A, Trope GE, Heathcote JG, Ethier CR. Deformation of the lamina cribrosa by elevated intraocular pressure. *Br J Ophthalmol.* 1994;78:643–648.
62. Sigal IA, Flanagan JG, Tertinegg I, Ethier CR. 3D Morphometry of the human optic nerve head. *Exp Eye Res.* 2010;90:70–80.
63. See JLS, Nicolela MT, Chauhan BC. Rates of neuroretinal rim and peripapillary atrophy area change: a comparative study of glaucoma patients and normal controls. *Ophthalmology.* 2009;116: 840–847.
64. Pederson JE, Anderson DR. The mode of progressive disc cupping in ocular hypertension and glaucoma. *Arch Ophthalmol.* 1980;98: 490–495.
65. Jonas JB, Fernandez MC, Sturmer J. Pattern of glaucomatous neuroretinal rim loss. *Ophthalmology.* 1993;100:63–68.
66. Tuulonen A, Airaksinen PJ. Initial glaucomatous optic disk and retinal nerve fiber layer abnormalities and their progression. *Am J Ophthalmol.* 1991;111:485–490.
67. Quigley HA, Addicks EM. Regional differences in the structure of the lamina cribrosa and their relation to glaucomatous optic nerve damage. *Arch Ophthalmol.* 1981;99:137–143.
68. Dandona L, Quigley HA, Brown AE, Enger C. Quantitative regional structure of the normal human lamina cribrosa: a racial comparison. *Arch Ophthalmol.* 1990;108:393–398.
69. Brown DJ, Morishige N, Neekhra A, Minckler DS, Jester JV. Application of second harmonic imaging microscopy to assess structural changes in optic nerve head structure ex vivo. *J Biomed Opt.* 2007;12:024029.
70. Jonas JB, Mardin CY, Schlotzer-Schrehardt U, Naumann GO. Morphometry of the human lamina cribrosa surface. *Invest Ophthalmol Vis Sci.* 1991;32:401–405.
71. Ogden TE, Duggan J, Danley K, Wilcox M, Minckler DS. Morphometry of nerve fiber bundle pores in the optic nerve head of the human. *Exp Eye Res.* 1988;46:559–568.
72. Girard MJ, Downs JC, Bottlang M, Burgoyne CF, Suh JK. Peripapillary and posterior scleral mechanics. Part II: experimental and inverse finite element characterization. *J Biomech Eng.* 2009;131:051012.
73. Girard MJ, Downs JC, Burgoyne CF, Suh JK. Peripapillary and posterior scleral mechanics-part I: development of an anisotropic hyperelastic constitutive model. *J Biomech Eng.* 2009;131:051011.
74. Downs JC, Suh JK, Thomas KA, Bellezza AJ, Burgoyne CF, Hart RT. Viscoelastic characterization of peripapillary sclera: material properties by quadrant in rabbit and monkey eyes. *J Biomech Eng.* 2003;125:124–131.
75. Schultz DS, Lotz JC, Lee SM, Trinidad ML, Stewart JM. Structural factors that mediate scleral stiffness. *Invest Ophthalmol Vis Sci.* 2008;49:4232–4236.
76. Spoerl E, Boehm AG, Pillunat LE. The influence of various substances on the biomechanical behavior of lamina cribrosa and peripapillary sclera. *Invest Ophthalmol Vis Sci.* 2005;46:1286–1290.
77. Siegwart JT Jr, Norton TT. Regulation of the mechanical properties of tree shrew sclera by the visual environment. *Vision Res.* 1999; 39:387–407.
78. Grytz R, Meschke G. A computational remodeling approach to predict the physiological architecture of the collagen fibril network in corneo-scleral shells. *Biomech Model Mechanobiol.* 2010;9:225–235.
79. Jonas JB, Fernandez MC. Shape of the neuroretinal rim and position of the central retinal vessels in glaucoma. *Br J Ophthalmol.* 1994;78:99–102.
80. Jonas JB, Budde WM, Nemeth J, Grundler AE, Mistlberger A, Hayler JK. Central retinal vessel trunk exit and location of glaucomatous parapapillary atrophy in glaucoma. *Ophthalmology.* 2001;108: 1059–1064.
81. Jonas JB. Trans-lamina cribrosa pressure difference (letter). *Arch Ophthalmol.* 2007;125:431; author reply 431.
82. Morgan WH, Yu DY, Alder VA, et al. The correlation between cerebrospinal fluid pressure and retrolaminar tissue pressure. *Invest Ophthalmol Vis Sci.* 1998;39:1419–1428.
83. Morgan WH, Yu DY, Cooper RL, Alder VA, Cringle SJ, Constable IJ. The influence of cerebrospinal fluid pressure on the lamina cribrosa tissue pressure gradient. *Invest Ophthalmol Vis Sci.* 1995; 36:1163–1172.
84. Burgoyne CF. A biomechanical paradigm for axonal insult within the optic nerve head. *Exp Eye Res.* First published on September 16, 2010 as doi:10.1016/j.exer.2010.09.005.

Appendix

Table A1. List of the Abbreviations and the Corresponding Full Names

Full Name	Abbreviations
95% Confidence interval	95%CI
Anterior laminar insertion	ALI
Anteriormost aspect of the subarachnoid space	ASAS
Anterior scleral canal opening	ASCO
Bruch's membrane	BM
Confocal scanning laser tomographic	CSLT
Early experimental glaucoma	EEG
EEG monkey both eyes perfusion fixed at 10 mm Hg	EEG 10/10
EEG monkey with control eye perfusion fixed at 10 mm Hg, treated eye at 30 mm Hg	EEG 10/30
EEG monkey with control eye perfusion fixed at 10 mm Hg, treated eye at 45 mm Hg	EEG 10/45
EEG eye perfusion fixed at 10 mm Hg	EEG 10
EEG eye perfusion fixed at 30 or 45 mm Hg	EEG 30/45
Difference that exceeded PIDmax and statistically significant	EPIDmax
Internal limiting membrane	ILM
Intraocular pressure	IOP
Lamina cribrosa	LC
Laser Diagnostics Technology	LDT
Mean position of the disc	MPD
Normal monkey both eyes perfusion fixed at 10 mm Hg	N 10/10
Normal monkey with one eye perfusion fixed at 10 mm Hg, other eye at 30 mm Hg	N 10/30
Normal monkey with one eye perfusion fixed at 10 mm Hg, other eye at 45 mm Hg	N 10/45
Normal eye perfusion fixed at 10 mm Hg	N10
Normal eye perfusion fixed at 30 or 45 mm Hg	N 30/45
Neural canal opening	NCO
Optic nerve head	ONH
Physiologic intereye difference	PID
Maximum physiologic intereye difference	PIDmax
Posterior laminar insertion	PLI
Post-NCO total prelaminar volume	PNCOTPV
Posterior scleral canal opening	PSCO
Spectral-domain optical coherence tomography	SDOCT
Topographic change analysis	TCA

Table A2. Magnitude of Experiment-wide Effects

Parameters	Normal Monkeys*				EEG Monkeys*				EEG Compliance‡§	
	Bilateral Normal Eyes Differences†		Normal Compliance†		Permanent Deformation†		Permanent Deformation Plus EEG Compliance†			
	N10(OD)-N10(OS)		N30/45-N10		EEG10-N10		EEG30/45-N10		(EEG30/45-N10)–(EEG10-N10)	
	Low	Upper	Low	Upper	Low	Upper	Low	Upper	Low	Upper
Neural Canal Architecture (μm)										
NCO Offset	−29	22	−17	41	−112	228	−13	63	−241	175
ASCO Offset	−23	29	−14	37	−4	69	1	66	−70	70
ALI Offset	−22	30	−13	39	−2	70	−4	61	−74	63
PLI Offset	−25	26	−2	50	***28***	***101***	***43***	***114***	−48	86
PSCO Offset	−27	35	−2	49	8	81	***35***	***100***	−46	82
ASAS Offset	−23	29	−4	47	***32***	***105***	5	71	−110	36
ASCO Depth	−5	9	−12	2	−6	14	−9	9	−23	15
ALI Depth	−5	9	−10	5	2	22	−22	−4	−44	−6
PLI Depth	−5	9	***−25***	***−10***	9	29	***−40***	***−21***	**−69**	**−30**‖
PSCO Depth	−3	11	***−30***	***−15***	0	21	***−55***	***−36***	**−76**	**−36**‖
ASAS Depth	**3**	**18**	−31	−17	−24	−3	***−80***	***−61***	**−77**	**−37**‖
ONH connective tissue (μm)										
Lamina cribrosa position	1	**8**	−3	3	***−104***	***−93***	***−72***	***−62***	**21**	**42**¶
Peripapillary sclera position	**−5**	**−1**	***13***	***17***	***12***	***17***	***44***	***50***	**27**	**38**‖
Lamina cribrosa thickness	**−7**	**−5**	***−13***	***−11***	***36***	***39***	***17***	***20***	**−22**	**−16**‖
Flange thickness	−8	2	−4	7	1	14	0	17	−14	16
Peripapillary sclera thickness	−1	6	−8	−1	***−17***	***−9***	−6	4	3	21
ONH laminar cupping (mm^3)										
Post-NCO total prelaminar volume	−0.089	0.069	−0.07	0.087	**0.096**	**0.319**	0.019	0.228	−0.3	0.132

* Data for the normal and EEG monkeys (the four leftmost data columns) are 95% CI for the difference between the compared groups of eyes (difference 95% CI) by ANOVA.

† In the four normal and EEG monkey data columns, bold values denote difference 95% CIs that achieve statistical significance by ANOVA ($P < 0.05$). Bold italic data denote a difference 95% CI that is not only statistically significant but is likely to be biologically significant, because it exceeds the difference 95% CI for bilaterally normal eyes.

‡ Data for EEG compliance are the lowest and highest possible differences between the 95% CIs for permanent deformation plus EEG compliance and permanent deformation. These data show the range of compliance in the high-IOP EEG eyes. Ranges that include 0 are not likely to be biologically important.

§ In the EEG compliance columns, the bold, underscored values are those that do not include 0 and exceed the difference 95% CI for normal compliance. These data indicate the magnitude of compliance change in the EEG 30/45 compared with the N30/45 eyes.

‖ The estimated EEG 30/45 eye compliance exceeded normal compliance for the following parameters: PLI, PSCO, ASAS depth (greater neural canal thinning, as demonstrated by decrease of canal depth), peripapillary scleral position (more posterior bowing), and LC thickness (less thickening).

¶ This 21- to 42-μm positive difference in anterior laminar position in the EEG 30/45 compared with the EEG 10 eyes not only suggests no overall laminar compliance (and therefore no laminar hypercompliance) in the EEG 30/45 eyes, but also less permanent deformation.

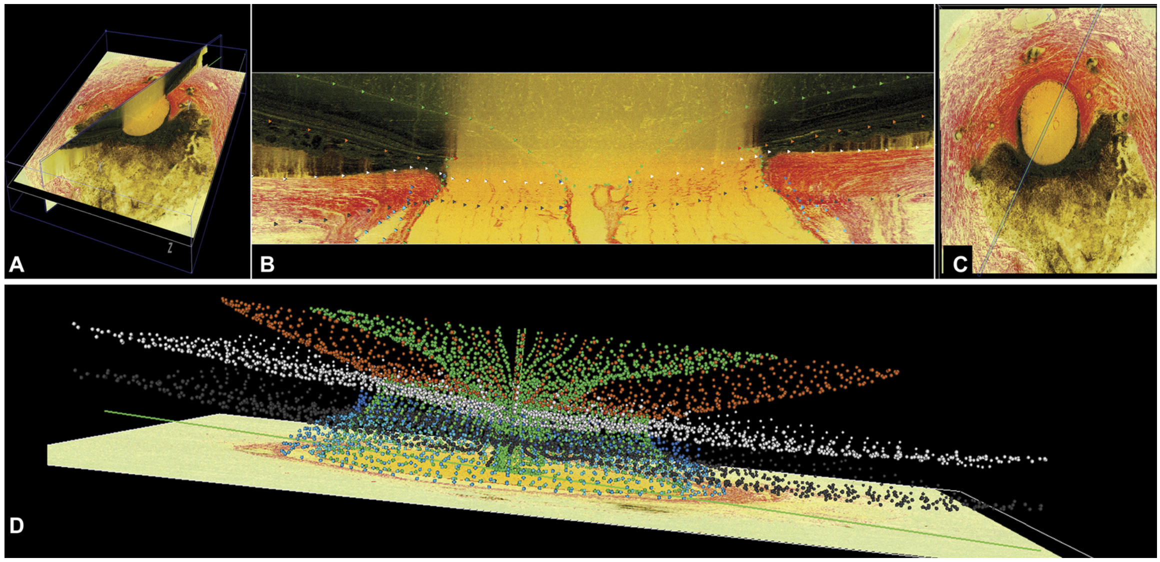

FIGURE A1. 3-D delineation in the colorized, stacked-section, 3-D ONH reconstruction of a single ONH. (**A**) Forty serial digital radial sagittal slices, each 7 voxels thick, were served to the delineator at 4.5° intervals. (**B**) A representative digital sagittal slice, showing all 13 landmarks which are 3-D delineated. Delineation was performed by using linked, simultaneous co-localization of the sagittal slice (shown) and the transverse section image through a given delineated point (**C**). (**D**) Representative 3-D point cloud showing all delineated points in a normal monkey ONH relative to the posterior serial section image (vitreous, *top*; orbital optic nerve, *bottom*).

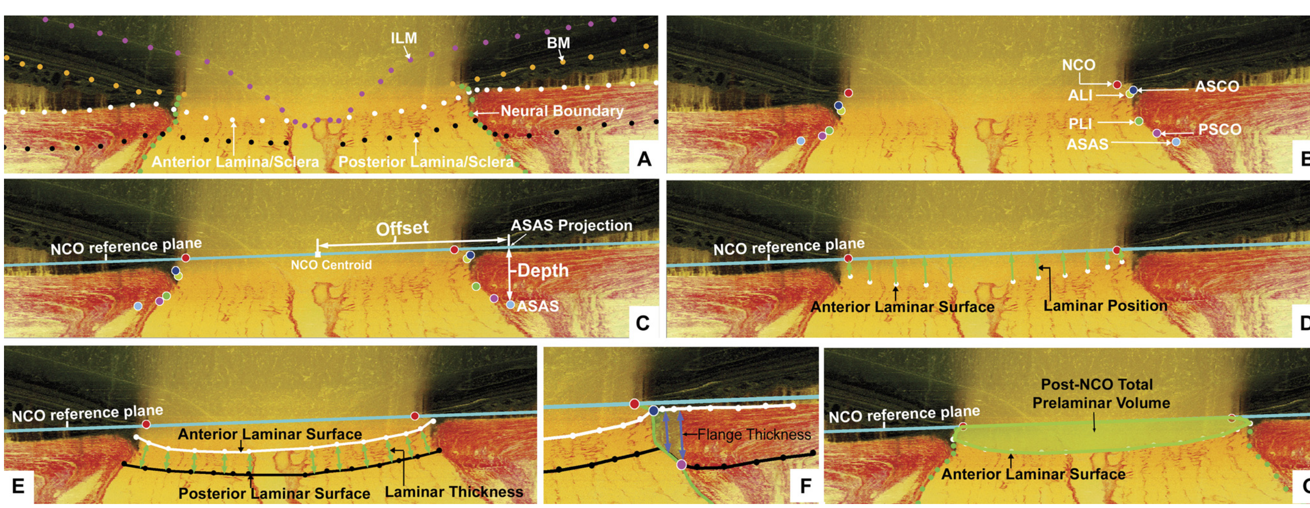

FIGURE A2. Parameter definitions. (**A**) A representative digital sagittal slice showing the internal limiting membrane (ILM, *pink dots*), Bruch's membrane (BM, *orange dots*), anterior laminar/scleral surface (*white dots*), posterior laminar/scleral surface (*black dots*), and neural boundary (*green dots*). (**B**) A representative digital sagittal slice showing neural canal architectures (abbreviations in Table A1). The neural canal includes the NCO (the opening in the Bruch's membrane/RPE complex, *red*), the ASCO (*dark blue*), the ALI (*dark yellow*, partly hidden behind the ASCO in *dark blue*), and the PLI (*green*), the PSCO (*pink*).The ASAS (*light blue*) was also delineated. (**C**) Definitions of the offset and depth using ASAS as an example. The rightmost ASAS point was projected to the NCO zero reference plane (*cyan line*), the distance between the NCO centroid and the projection of ASAS is defined as *offset*. The distance between the ASAS to the projection is defined as *depth* of ASAS. The offset and depth of all other neural canal architectures were defined in the same way: (**D**) Laminar position (*green arrow*), the shortest distance from the delineated anterior laminar surface point (*white dot*) to the NCO zero reference plane. (**E**) LC thickness, determined at each delineated anterior surface point by fitting a continuous surface (*white line*) to all anterior surface points and then measuring the distance along a normal vector of the anterior surface (*green arrows*) from each anterior delineated point to the posterior surface. (**F**) Thickness of the scleral flange at each delineated anterior surface point (*white dots*), the distance between the neural canal boundary points (*green line*) along a vector parallel to the PSCO normal vector (*blue arrows*). (**G**) PNCOTPV (*light green*: a measure of the laminar or connective tissue component of cupping), the volume beneath the NCO zero reference plane (*cyan line*), above the LC and in the neural canal wall.

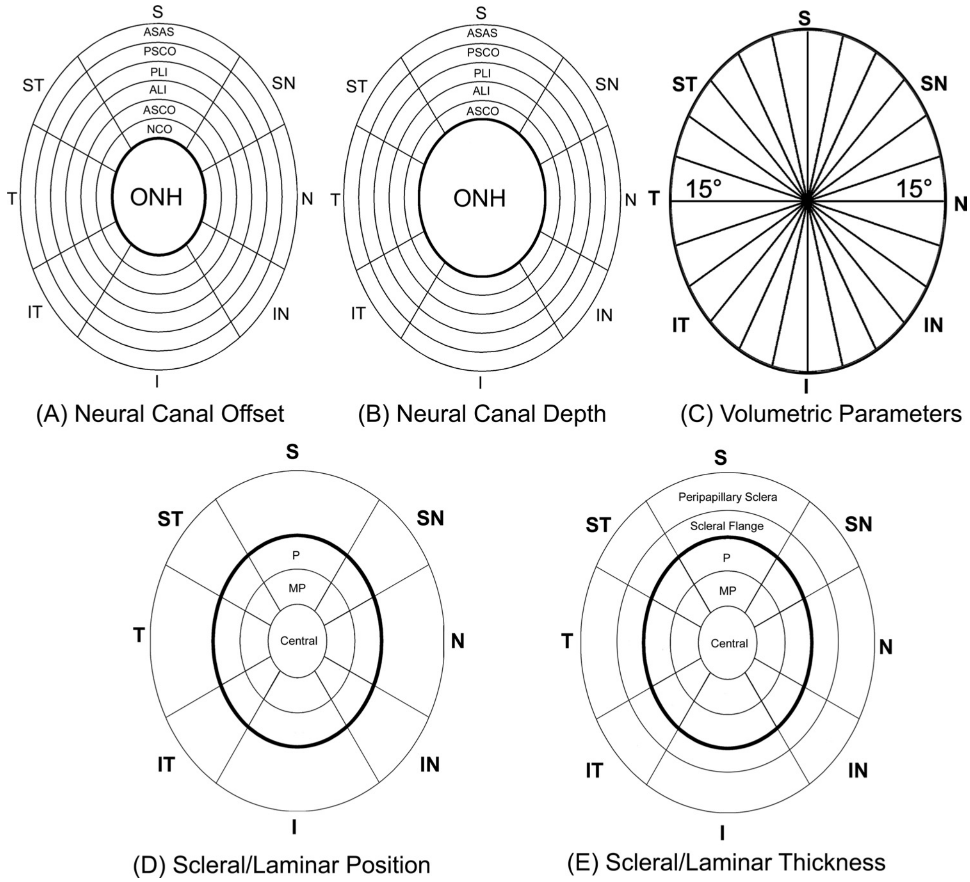

FIGURE A3. Parameter regionalization (right-eye configuration). Neural canal offset (**A**) and depth data (**B**) for each neural canal landmark were pooled for eight anatomic regions; superior (S), superonasal (SN), nasal (N), inferonasal (IN), inferior (I), inferotemporal (IT), temporal (T), and superotemporal (ST). The S, N, I, and T regions contained all marks in 60° sections of the ONH centered about the S–I and N–T clinical axes, and the SN, IN, IT, and ST regions contained all marks in 30° radial sections of the ONH centered about the SN–IT and IN–ST axes. Concentric rings represent the different neural canal landmarks from the ONH internal entrance NCO to its external exit PSCO, as shown in the superior regions in (**A**) and (**B**). Neural canal depth measurements start with the ASCO rather than the NCO. (**C**) From the center of the NCO, 12 radial sections perpendicular to the NCO zero reference plane divided the volumetric parameters into 24, 15° radial regions. Regional volumes were projected onto the NCO zero reference plane, color coded by region and overlaid onto a standard ellipse. (**D**) In the lamina (regions inside the *bold line*), position data were pooled into 17 regions according to the three radial regions (central; MP, middle periphery; P, periphery) and eight quadrants, as in (**A**) and (**B**). Peripapillary sclera (regions outside the *bold line*) position data were pooled into eight regions (inner boundary, starting from the ASCO ellipse (bold line) to an ellipse with a size that is 1.62 times that of the ASCO ellipse. (**E**) In the lamina (regions inside *bold line*), thickness data were pooled into 17 regions as laminar position data in (**D**). Peripapillary scleral thickness data were pooled into 16 regions two radial regions (scleral flange thickness, covers area from ASCO to PSCO; peripapillary sclera region, inner boundary starting from PSCO to an ellipse with a size that is 1.62 times that of the ASCO ellipse).